NIS-GCR-95-678

A STUDY OF TWO PHASE HIGH LIQUID LOADING JET FIRES

R. Wade, Y.R. Sivathanu and J.P. Gore

School of Mechanical Engineering
Purdue University
West Lafayette, IN 47907-1077
October 1995

U.S. Department of Commerce
Ronald H. Brown, *Secretary*
Technology Administration
Mary L. Good, *Under Secretary for Technology*
National Institute of Standards and Technology
Arati Prabhakar, *Director*

Notice

This report was prepared for the Center for Fire Research of the Building and Fire Research Laboratory of the National Institute of Standards and Technology, under Grant Number 60NANB3D1441. The statements and conclusions contained inthis report are those of the authors and do not necessarily reflect the views of the National Institutes of Standards and Rechnology, the Building and Fire Research Laboratory, and the Center for Fire Research.

A STUDY OF TWO PHASE HIGH LIQUID LOADING JET FIRES

by

R. Wade, Y. R. Sivathanu and J. P. Gore
Thermal Sciences and Propulsion Center
School of Mechanical Engineering
Purdue University
West Lafayette, IN 47907-1077

Prepared for

U. S. DEPARTMENT OF COMMERCE
NATIONAL INSTITUTE OF STANDARDS AND TECHNOLOGY
CENTER FOR FIRE RESEARCH
BUILDING AND FIRE RESEARCH LABORATORY

NIST GRANT NUMBER: 60NANB 3D1441
Annual Report for the Period: 9/1/1993- 8/30/1994

Dr. David D. Evans
NIST Scientific Officer

A STUDY OF TWO PHASE HIGH LIQUID LOADING JET FIRES

by

R. Wade, Y. R. Sivathanu and J. P. Gore
Thermal Sciences and Propulsion Center
School of Mechanical Engineering
Purdue University
West Lafayette, IN 47907-1077

Sponsored by

U. S. DEPARTMENT OF COMMERCE
NATIONAL INSTITUTE OF STANDARDS AND TECHNOLOGY
CENTER FOR FIRE RESEARCH
BUILDING AND FIRE RESEARCH LABORATORY

A STUDY OF TWO PHASE HIGH LIQUID LOADING JET FIRES

April 1995

Sponsored by:

U. S. Department of Commerce
National Institute of Standards and Technology
Building and Fire Research Laboratory
Center for Fire Research

A STUDY OF TWO PHASE HIGH LIQUID LOADING JET FIRES

Executive Summary

A study of high liquid loading spray jet fires simulating fuel pipe leaks, tank ruptures, and oil well blowouts is in progress. Measurements of liquid drop sizes, flame heights, radiative loss fractions, evaporation lengths, and path integrated transmittances and emission temperatures have been completed for over 20 flames burning toluene and crude oil with 5-25% by mass of atomizing methane and 5-13% mass of stabilizing hydrogen.

Measurements of flame heights showed significant effects of two phase flow. For example, the flame height increased almost linearly with increasing heat release rate in an apparently forced flow regime. Furthermore, the lowest methane loading flames are found to be longest instead of shortest as predicted by existing correlations. The changes in flame heights can be as much as 50%. Measurements of radiative loss fractions for the toluene flames showed that increase with heat release rate, decrease with heat release rate and invariance with heat release rate are all possible depending upon the exact coupling between soot formation, radiative heat loss and soot oxidation. Effects of atomizing methane mass flow rate on sooting tendency were found to be significant while those of flame stabilizing hydrogen were found to be surprisingly small.

Measurements of local soot volume fraction statistics using statistical tomography show a bimodal probability density function with soot streaks occuring in an intermittent fashion for flames with high sooting tendency. The soot streaks disappear for flames with high methane loading that contain relatively small quantities of soot.

Research involving scaleup of the high liquid loading burner to 500 kW heat release rates is recommended. Measurements of flame heights, radiative loss fractions, soot volume fractions, temperatures, and entrainment rates will be completed in an attempt to understand the behavior of high liquid loading spray flames.

The work is establishing the basic physical processes important in high liquid loading spray jet fires. The results are of value in predicting hazard from liquid storage tank and transport line rupture fires and safe distances for layout of plant and equipment around such devices. Improvements in this area will ultimately reduce the fire loss and insurance and litigation costs for the US industry.

Table of Contents

LIST OF FIGURES

CHAPTER 1 : GLOBAL PROPERTIES OF HIGH LIQUID LOADING SPRAY FIRES

1.1 INTRODUCTION

Large scale industrial fires result from rupture of liquid storage tanks , transport pipe lines, and oil well blowouts in petrochemical industry. These fires represent a serious hazard to personnel. They may also result in a large cost penalty in terms of insurance, litigation, interruption of service, loss of sales, and replacement of plant and equipment. Well head fires after the liberation of Kuwait serve as a high visibility reminder of the possibility of the stabilization of high liquid loading jet flames. Evans and coworkers (1991) attempted to gather scientific data concerning the fires in Kuwait. However, measurements under those conditions must be limited to a few global properties which can be interpreted by controlled laboratory studies.

Effective atomization of a liquid fuel with minimal amount of dissolved gases occurs when a two phase mixture expands from a relatively high pressure source into the atmosphere. This principle was used in the construction of an effervescent atomizer-burner during an earlier NIST sponsored grant in this laboratory (Dutta et al., 1994). Prior to the development of this burner, only one laboratory study of high liquid loading jet fires was reported (Hustad and Sonju, 1986). These investigators mixed oil and gas in a chamber upstream of relatively large (10-33 mm diameter) nozzles. Jet flames were stabilized at the exit of the nozzles under attached as well as lifted flame conditions. Heat release rates varied between 1-8 MW. Hustad and Sonju (1986) showed that the two phase flames are much longer than gaseous flames with the same heat release rate. A correlation based on an adjustment to the entrainment rate due to changes in the jet fluid density was devised using the flame length data. The experiments of Hustad and Sonju (1986) involved conditions closer to accidental fires in which control of the atomization quality can not be attained. The relatively large size of the fires also prevented a detailed study of the flow field, temperatures, soot volume fractions, and atomization quality. The resulting flame length correlation accounted for the two phase density but did not account for effects that may result from the quality of atomization and the initial dispersion of the fuel caused by convective drop transport.

The proposed work is partly motivated by the findings of Dutta et al. (1994) regarding global properties of high liquid loading crude oil +methane+hydrogen jet fires. This work showed that two phase flow effects affected the flame lengths and radiative fractions of such fires significantly. Dutta et al. (1994) measured visible flame lengths, radiative heat loss fractions and emission temperatures, as well as visible transmittance. The visible flame length measurements showed that decreasing the methane to liquid mass ratio (MLR) leads to an increase in flame length for a fixed total heat release rate. Increase in heat release rate at a fixed MLR also leads to increase in flame length. Based on a comparison with the correlation reported by Hustad and Sonju (1986) for two phase fires, the above effects could not be explained. The correlation predicted that the lowest MLR flames should be the shortest while the experiments showed these to be the longest. The correlation predicted that the flame lengths should be independent of heat release rates, while the experiments showed an increase with increasing heat release rates. The measurements of radiative heat loss fractions completed by Dutta et al. (1994) showed a large variation (increase from 10% to 20% for a decrease in MLR from 20% to 5%) with MLR. However, the radiative heat loss fractions were almost constant over the range of heat

release rates for a fixed MLR. The measurements of emission temperatures and transmittance showed that the differences in radiative loss fractions result from the differences in sooting tendency for different MLRs. Significant reduction in combustion efficiency as a cause for the increased radiative loss fractions was considered improbable based on the high measured emission temperatures.

1.2 MEASUREMENTS OF GLOBAL PROPERTIES

1.2.1 SUMMARY

The evaporation length measurements for the flames studied by Dutta et al. (1994) have been completed as discussed by Swan et al. (1994) and in section 1.2.3. Flame lengths and radiative heat loss fractions for 19 spray flames burning toluene with methane and hydrogen have been measured to assess the effects of fuel type on the high liquid loading spray flame characteristics. Consideration of a larger number of operating conditions was prompted by the differences in the behavior of the radiative loss fraction with MLR as discussed in section 1.2.3 as well as the significant observed effects of the hydrogen flow rate on sooting tendency. Path integrated temperatures and transmittance at 632 nm for five representative flames out of the 19 selected to delineate the effects of hydrogen to liquid ratio (HLR), MLR, and heat release rates have been measured using an emission/absorption instrument developed in this laboratory. The momentum rate at the atomizer/burner exit is being measured using a force balance probe for all 19 flames in order to determine the forced/buoyant regime for consideration of the flame length correlation. The entrainment velocities for the five representative flames will be measured during the current grant period. The drop sizes have been measured previously in cold sprays with a Malvern instrument.

The measurements have shown that, although evaporation lengths in the high liquid loading spray flames do vary with atomization quality, within the range of the operating conditions of the present experiments, these variations are not large enough to account for the observed changes in flame length. Measurements of path integrated soot and emission temperatures suggest that changes in flame visibility resulting from changes in these properties may account for a part of the variation in the visible flame lengths. The radiative heat loss fraction is reduced significantly by an increase in MLR while changes in HLR did not affect the radiative loss fraction significantly. This some what surprising effect needs to be investigated further with detailed local soot volume fraction and emission temperature data. Indications are that the high momentum rate associated with the methane flow interferes with the soot formation process in the spray flame. However, the extent to which this effect is unique to spray flames needs to be examined.

1.2.2 EXPERIMENTAL METHODS

The effervescent atomizer burner designed for the simulation of high liquid loading jet fires has been described before (Dutta et al., 1994). A sketch of this burner is shown in Fig. 1 for completeness. The liquid fuel flows into an annular space formed by the body of the burner and the central atomizing gas injection tube. The atomizing gas (methane in the flames studied to date) is injected through multiple holes in the central tube. In order to stabilize the flame on the burner port, a ring flame is established by injecting hydrogen near the burner orifice. The two-phase (liquid fuel plus atomizing

methane) flow exits the central 0.18 mm orifice and flows through the ring flame which helps establish a jet flame attached to the 4.76 mm diameter exit port of the burner. The top plate of the burner is cooled by a small flow of water flowing through an annular space to avoid fuel coking near the orifice.

The flow metering and control system for the effervescent atomizer/burner has been described in detail by Dutta et al. (1994). Briefly, the flow rates of the liquid fuel, the atomizing methane, and the pilot-flame hydrogen are metered using calibrated rotameters and controlled using metering valves. The pressure of the methane stream and the liquid fuel stream just upstream of the burner are monitored using gauges. The system consists of two separate sets of shutoff valves for each fuel. The liquid fuel is pressurized by storing it in a pressure vessel and admitting nitrogen at a desired pressure into the ullage space. The pressure in the liquid fuel tank is maintained constant by a pressure regulator in the nitrogen line.

During operation, the hydrogen flow is started first and a pilot flame is established. The methane flow is started next and a gaseous jet flame is stabilized. Finally, the liquid flow is initiated and controlled at the desired operating conditions. After several minutes of startup transients, the system stabilizes to produce a two phase jet fire with relatively high mass loading of the liquid fuel. Unburnt/unevaporated liquid fuel does not escape the flame/burner system under normal operating conditions.

Figure 2 shows the Mie scattering system used to measure the distance up to which liquid fuel in significant quantity exists along the axis of the spray flame. The Mie scattering instrument consists of an Argon ion laser, a chopper and a mirror for directing the beam through the flame axis into a beam stop. The light scattered by the liquid droplets at right angle to the beam direction is collected an focused by a pair of lenses into the aperture of a photomultiplier tube that defines the size of the probe volume over which the drops are measured. In the present apparatus, a probe size of 4 mm diameter was obtained. The output voltage generated by the PMT is proportional to the intensity of the scattered light which depends on the drop number density and drop size in the spray flame. Since both these quantities decrease due to evaporation in the spray flame, the voltage output of the PMT can be used to detect the location beyond which most of the liquid.

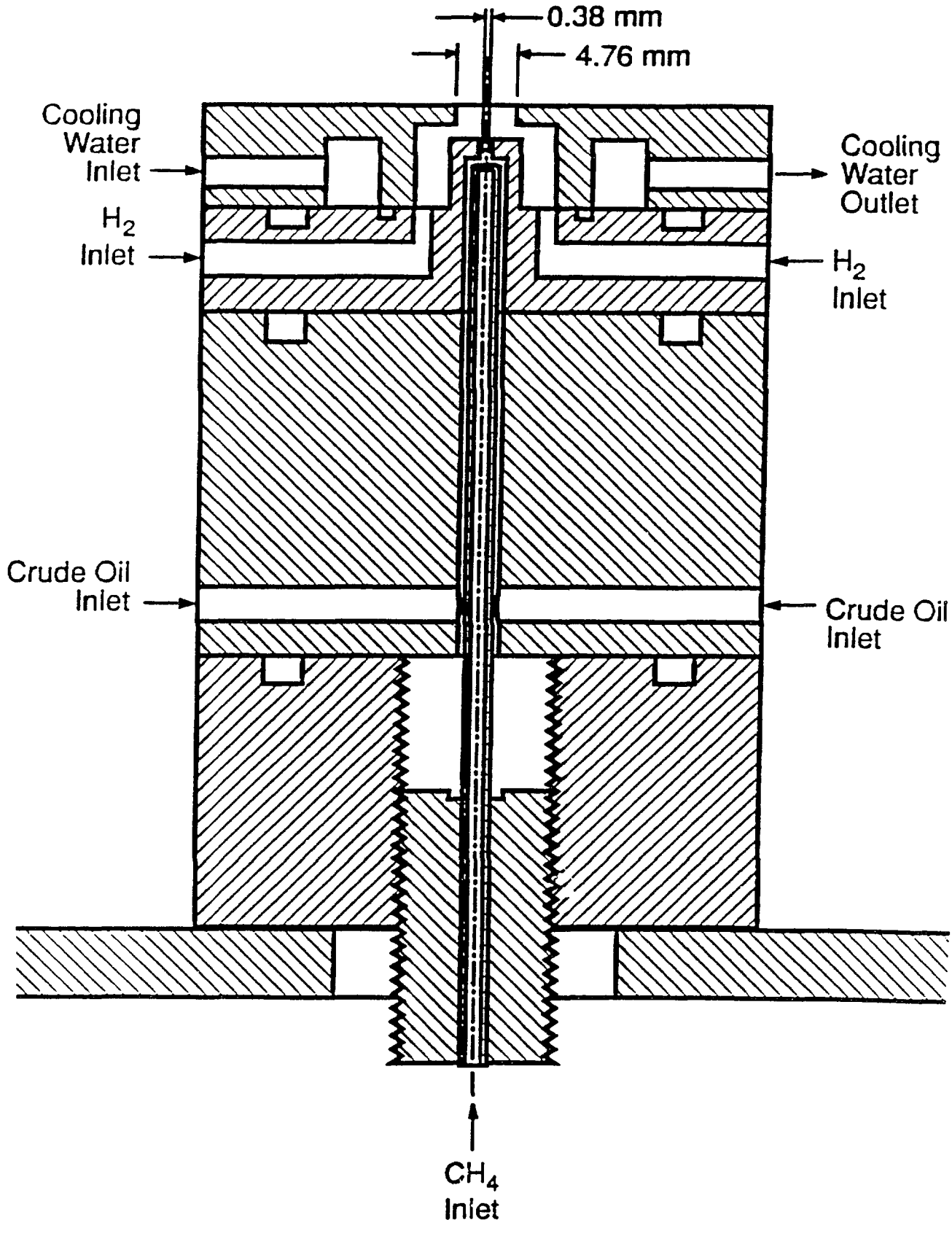

Figure 1. Sketch of the effervescent atomizer-burner.

MIE-SCATTERING ARRANGEMENT

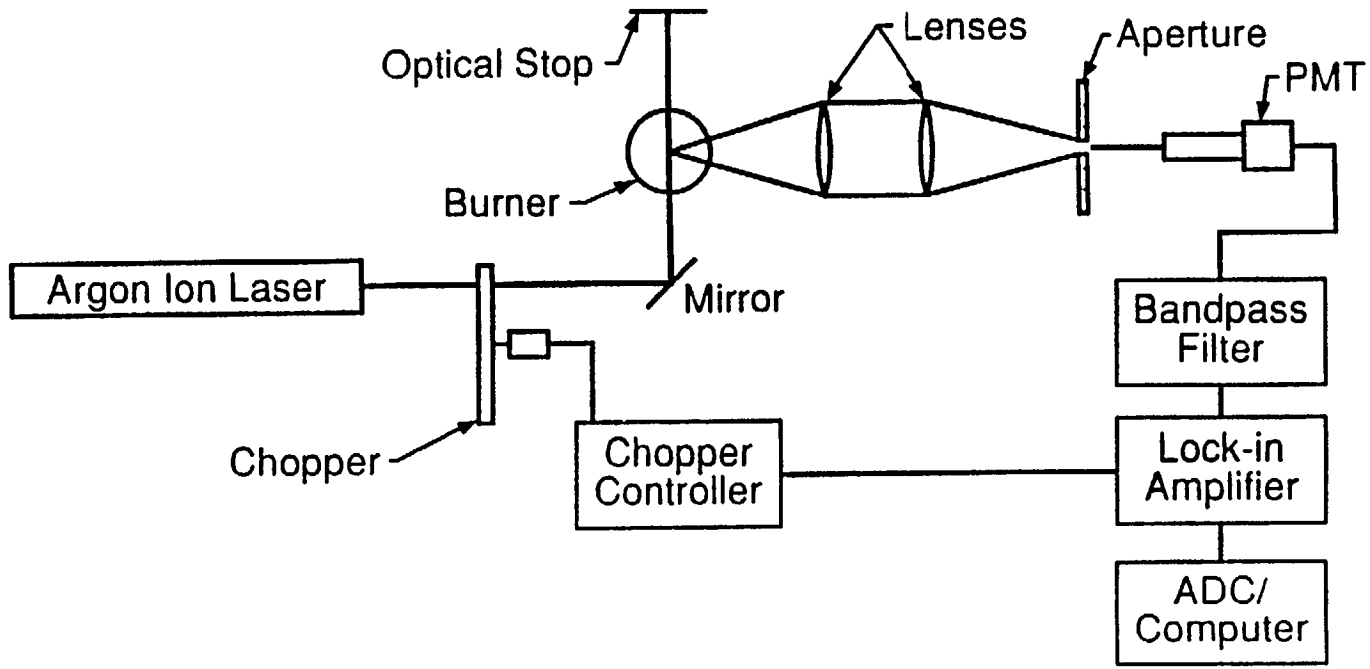

Figure 2. A schematic of the Mie scattering instrument used for evaporation length measurements.

drops have evaporated. The evaporation lengths of the crude oil+methane+hydrogen flames studied by Dutta et al. (1994) were obtained using the Mie scattering instrument.

Table 1 shows the operating conditions for the crude oil +methane+ hydrogen flames studied by Dutta et al. (1994). The mass flow rate of the atomizing methane varied between 5 and 20 % of the mass flow rate of the crude oil). The hydrogen flow used for flame attachment did not affect the atomization quality significantly and was maintained at 16.4 mg/s for all the flames except the last. In order to stabilize the flame with the highest crude oil flow, a higher flow of hydrogen (21.2 mg/s) was required. The heat release rates for the flames varied between 9 and 21 kW based on nominal heating values of 43400 kJ/kg for the crude oil, 50000 kJ/kg for methane, and 120900 kJ/kg for hydrogen. The Reynolds number characteristic of the jet can be evaluated based on the external orifice diameter (4.76 mm) on which the flame is stabilized or based on the diameter through which the two-phase material exits (0.18 mm). The use of the larger diameter assumes that the material expands to fill the exit port while the use of the smaller diameter assumes that the jet is formed independent of the external orifice. The two different assumptions lead to Reynolds numbers differing by two orders of magnitude.

Toluene flames were selected next in view of the wide industrial use of this material as a solvent. Further more, the high sooting tendency of this fuel allows an assessment of whether the results concerning reduction in radiative heat loss and soot formation observed for effervescent atomized crude oil flames are associated with the burner configuration.

A total of 19 flames were studied in terms of their flame height and radiative heat loss fractions. The operating conditions for these flames are summarized in Table 2. As seen from Table 2, the first five flames are designed to study the effects of changing the methane to liquid ratio (MLR). Therefore, these flames have a fixed hydrogen to liquid mass flow rate (HLR) and a fixed total heat release rate of 10 kW including the heat release rates of toluene, methane and hydrogen. The next five flames show the effect of MLR for identical HLR for flames with a heat release rate of 15 kW. The next three flames have identical HLR as the first two sets with increasing MLR at a fixed heat release rate of 20 kW. The next two flames have a total heat release rate of 25 kW and can be studied for two different MLRs with identical HLRs. The last four flames are selected to study the effects of a much lower hydrogen flow rate on the flame properties by fixing the HLR at 5% and selecting the four flames that are stable at this low HLR.

Table 1: Operating Conditions.

Test Case	$\dot{m}_{OIL}$ (mg/s)	$\dot{m}_{CH_4}$ (mg/s)	$Re_{d = 4.76\ mm}$	$Re_{d = 0.38\ mm}$	Q_f (kW)	X_R (%)
1.	135	27.0	3.8×10^3	1.8×10^4	9.2	11.4
2.	234	32.8	5.5×10^3	2.3×10^4	14.2	10.2
3.	238	23.8	4.9×10^3	1.8×10^4	13.5	15.5
4.	250	25.0	5.1×10^3	1.9×10^4	14.0	14.0
5.	260	13.0	4.8×10^3	1.1×10^4	13.9	21.4
6.	328	16.4	5.4×10^3	1.3×10^4	17.0	20.7
7.	360	18.0	5.7×10^3	1.5×10^4	18.5	20.6
8.*	400	20.0	6.9×10^3	1.6×10^4	21.0	19.5

*HIGHER HYDROGEN FLOW RATE

$$Re_d = \frac{\rho_{TP}\, V_{TP}\, d}{\mu_{TP}}$$

Table 2: A Summary of Operating Conditions for the toluene+methane+hydrogen flames.

Q_f , kW	MLR %	HLR %	Tolune, mg/s	H_f, cm
10	5	13	172	45
10	10	13	165	44
10	15	13	158	40
10	20	13	152	38
10	25	13	147	34
15	5	13	258	54
15	10	13	247	50
15	15	13	238	45
15	20	13	228	42
15	25	13	220	38
20	5	13	344	59
20	10	13	330	52
20	15	13	317	49
25	5	13	430	64
25	10	13	412	55
10	5	5	206	40
10	10	5	196	39
15	5	5	310	48
20	5	5	413	54

1.2.3. RESULTS AND DISCUSSION

Crude Oil Flames

Evaporation Lengths

Figure 3 shows a graph of the mean voltage recorded by the PMT used for measuring the intensity of light scattered by the drops (and soot particles) in the flame as a function of axial distance. The evaporation length was defined as the axial location at which the scattering signal from the drops reduced to a background value of approximately 0.1 Volts from its peak value in the 2 to 3 Volts range at the injector exit. A complete scan of the visible flame region showed that the scattered light signal decreased to this low value and remained low for a considerable distance and then started increasing again due to scattering by soot particles. Finally, the scattering from soot particles decreased as their concentration decreased by oxidation and mixing with surrounding air. However, the evaporation length could be measured in spite of the possible interference from soot particles due to the two distinct regions in which drops and soot exist along the axis. The width of the evaporation zone could not be determined using the present technique since drops and soot could co-exist at a location along the radial direction where the evaporation is complete. The polarized light scattering technique would address this issue. However, a higher laser power is required for this technique as discussed before.

Attention was focused on the drop evaporation region next in order to determine the evaporation lengths for the seven flames studied by Dutta et al. (1994). Figure 4 shows the scattered light intensity plotted as a function of axial distance for three flame with a fixed MLR of 5% and heat release rate varying from 14 kW to 19 kW. The evaporation length for the flame with the highest heat release rate is larger by approximately 2 injector diameters. This is probably due to the larger drop sizes produced by the nozzle under these conditions. The higher value at a location very close to the nozzle exit also suggests that the initial drop sizes for this case are relatively large. The flame with 17 kW heat release rate also shows a higher scattered light intensity at the injector exit. However, the evaporation length for this flame appears to be very close to that for the 14 kW flame. Thus the evaporation length for the flames vary between x/d=10 and 12 for the three 5% MLR flames.

The effects of MLR on the evaporation length are shown in Fig. 5 for all the flames studied by Dutta et al. (1994). It is clearly observed that the evaporation lengths decrease with MLR. For a fixed MLR, the evaporation lengths for a high heat release rate flame can be as much as a factor of 2 higher than those for a low heat release flame. There is also a factor of 2 change with MLR. However, the evaporation lengths for all of the flames considered here are between 7 and 14 diameters. The variation is in the same direction as the changes in flame length in that the longest visible flames also have the longest evaporation length. However, the evaporation length itself is much smaller than the visible flame length for these flames. Hence, changes in the evaporation lengths can not completely account for the variations in the visible flame lengths for the present atomizer performance.

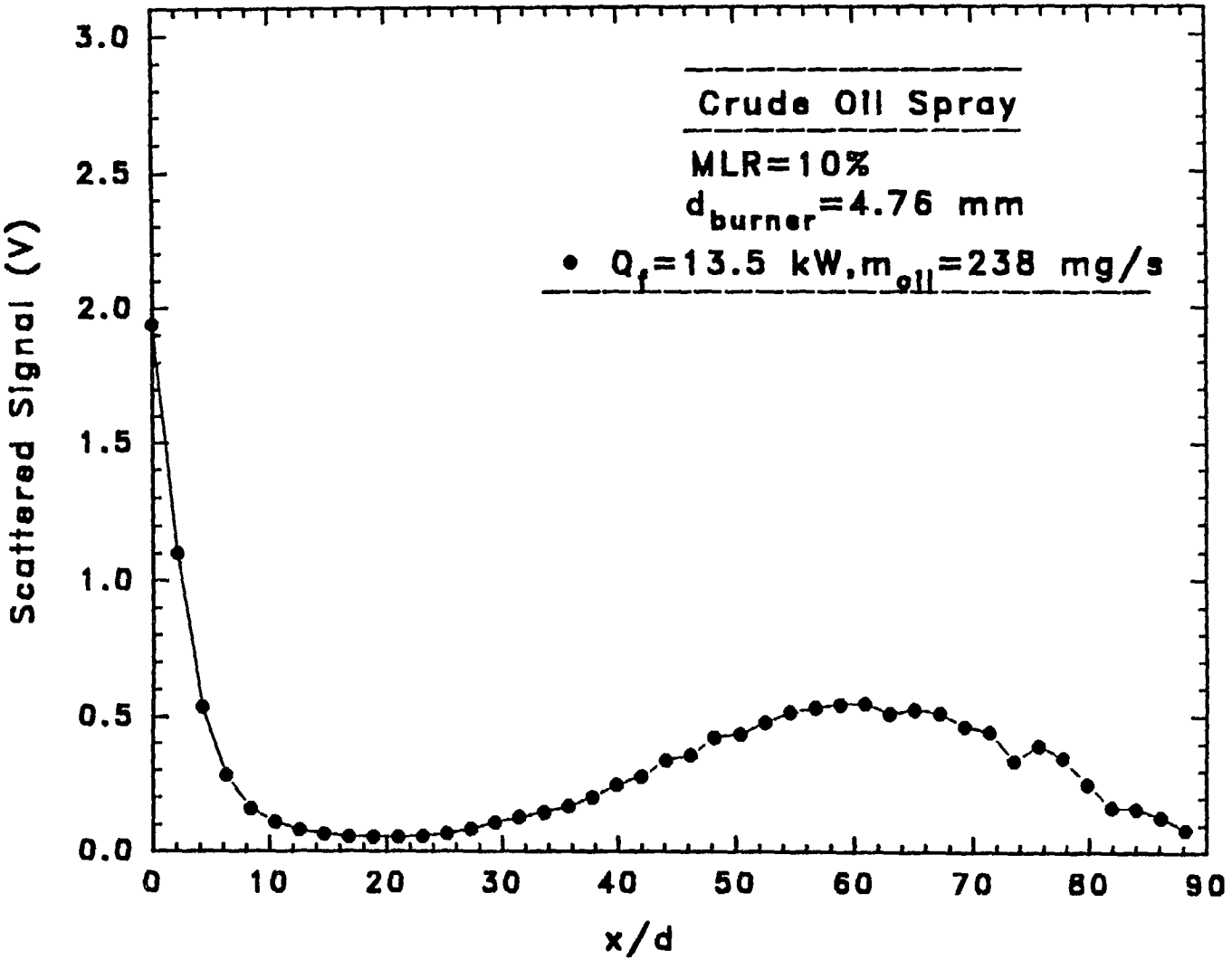

Figure 3. Voltages measured by the scattered light detection PMT as a function of normalized axial distance along the axis of MLR=10%, Q_f =13.5 kW Alberta sweet crude oil + methane+hydrogen jet fire.

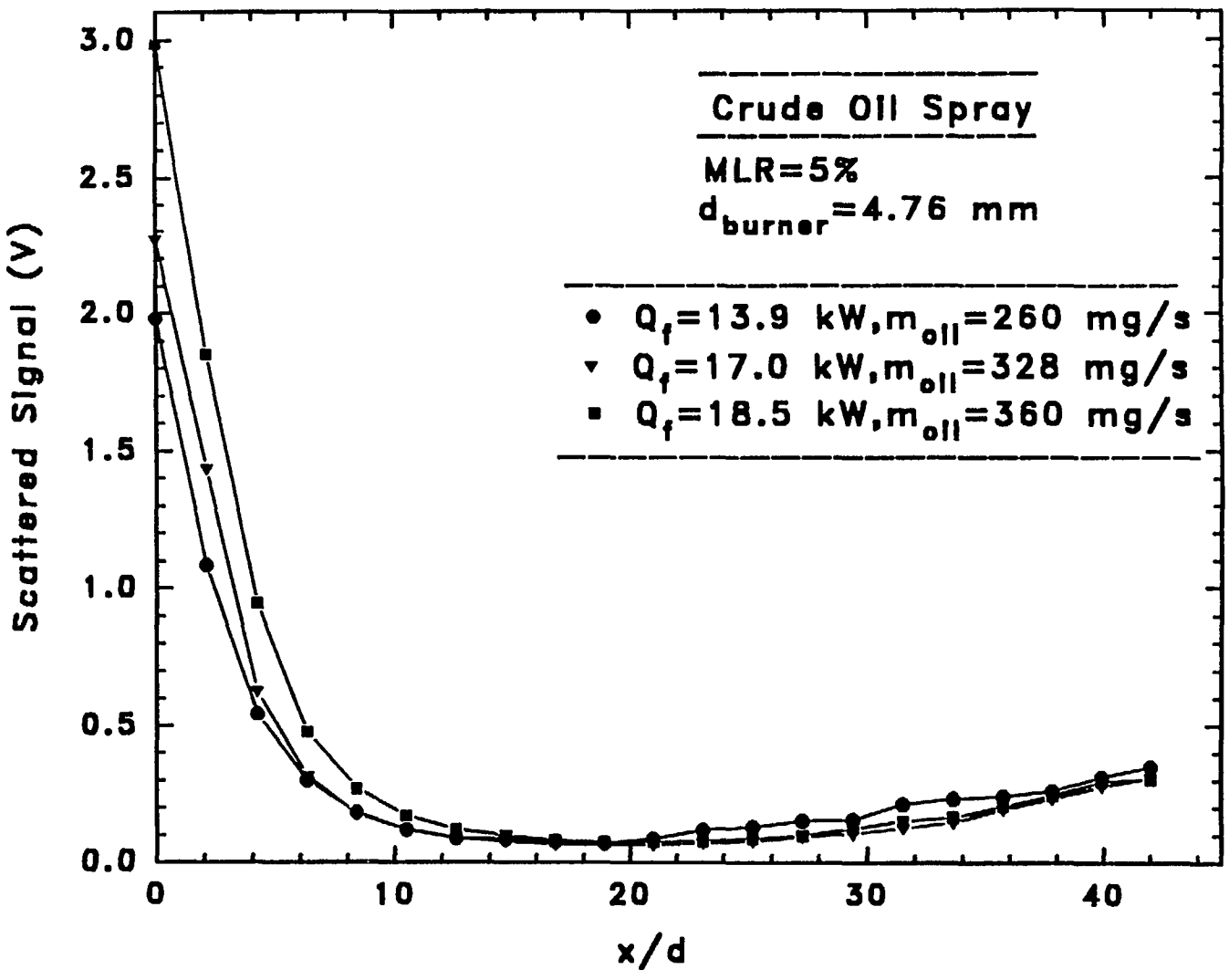

Figure 4. Voltages measured by the scattered light detection PMT as a function of normalized axial distance along the axis of three MLR=5 % Alberta sweet crude oil + methane+hydrogen jet fires with three different Q_f.

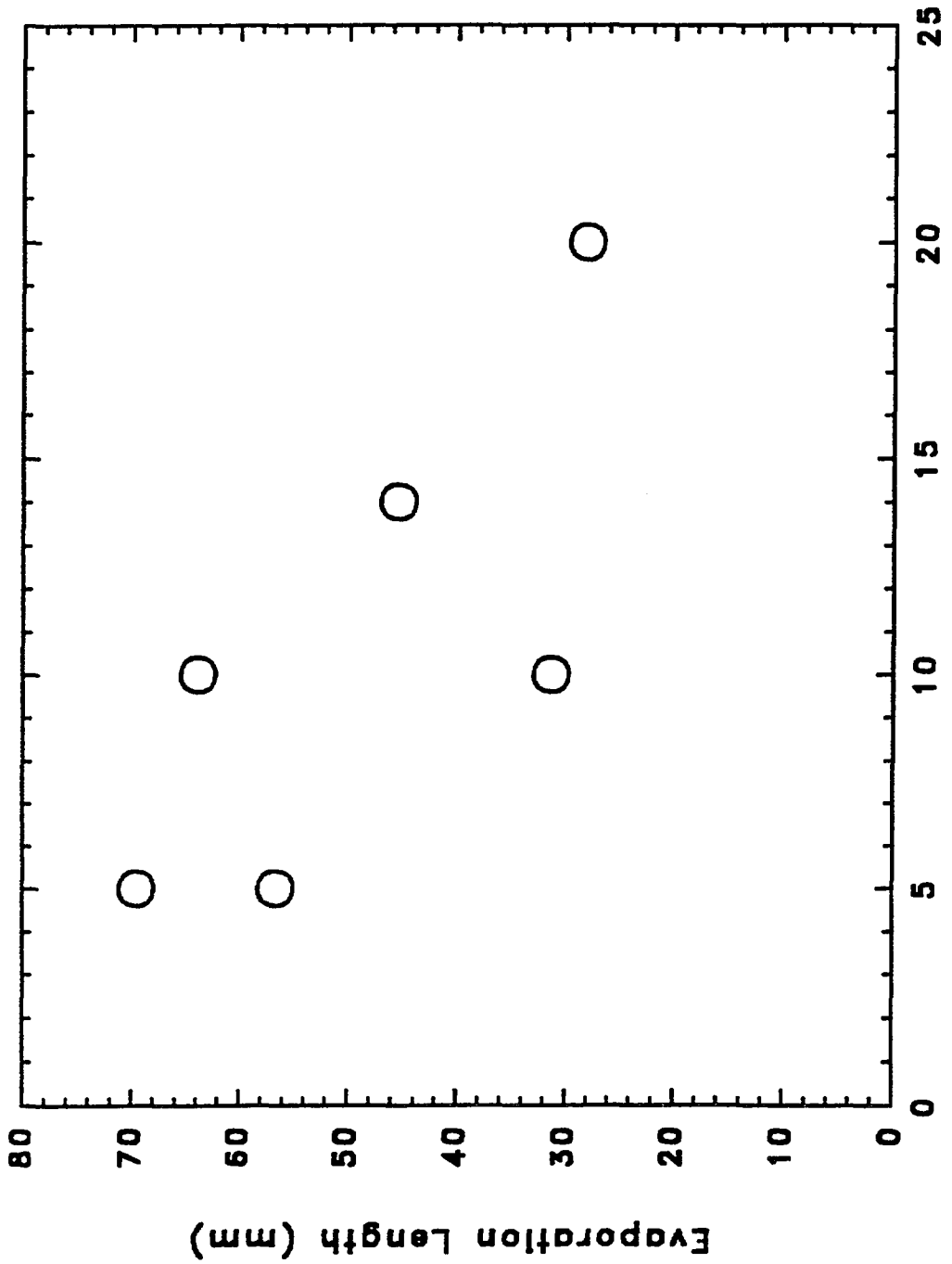

Figure 5. Measurements of evaporation lengths for all the crude oil jet fires as a function of MLR.

It is important to recognize that the above conclusion regarding the importance of the evaporation length in determining the flame length is highly dependent on the atomizer performance. During the course of the experiments, the atomizer occasionally got partially clogged with small stray particles under these conditions, many large drops escaped the primary evaporation zone and drops evaporated and burnt throughout the visible flame zone. Thus, with poorer atomizer performance the visible flame length and the evaporation lengths could even be equal.

Toluene Flames

Evaporation Lengths

The evaporation length measurements for the crude oil+methane+hydrogen flames described above showed that although the evaporation lengths increase with increasing firing rate and decreasing MLR by up to a factor of two, the dependence of flame heights on evaporation lengths can not be substantial for the present burner since the evaporation lengths are much smaller (less than 2 %) of the flame height. Substantial increase in firing rate and changes in the volatility of the fuel may change this conclusion. However, for the present experiments, the effects of changes in evaporation lengths can be considered less important than other possible effects. Hence, these effects are being considered first.

Flame Heights

Figure 6 shows the flame height "H_f" normalized by the external orifice diameter "d" (4.76 mm) plotted as a function of total heat release rate for the 19 flames in Table 2. As seen in Fig. 6, the flame height increase with increasing heat release rate for all the conditions studied. For the lowest MLR of 5 %, the flame height increases by approximately 40% with an increase in heat release rate from 10 to 25 kW. For flames with higher MLR, the increase in flame length with increase in heat release rate is less than that for MLR=5%. At a fixed heat release rate, the flame height decreases with increasing MLR for all of the conditions studied. The filled symbols in Fig. 6 show that the flame height decreases with decreasing HLR. This result is somewhat contrary to expectation but has been observed consistently. Measurements of emission temperature and transmittance reported later in this document, shed some light on this issue and highlight the importance of radiative cooling in the reduction of the visible flame length.

Similar to the finding of Dutta et al. (1994), the correlation for flame height from the literature are not capable of predicting the present experimental results shown in Fig. 6.

Radiative Heat Loss Fractions

The radiative heat loss fractions (X_R) for the 19 flames were measured using the single point technique of Sivathanu and Gore (1993). The radial distance of the radiometer from the flame axis was selected to be equal to flame height H_f and the height of the radiometer from the burner exit was selected to be $H_f/2$ in accordance with the single point technique. The radiative heat flux measured by the calibrated radiometer placed at this location was multiplied with the area

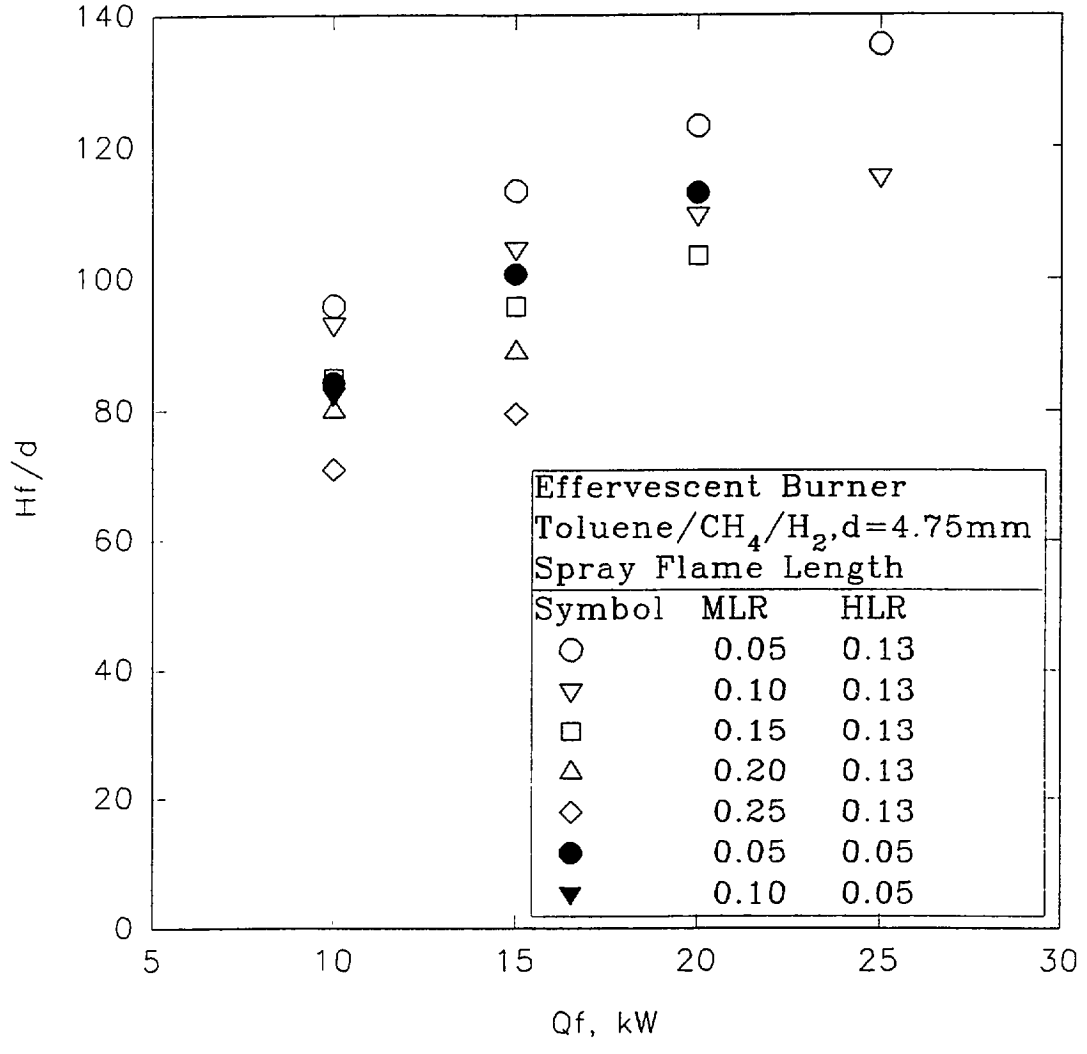

Figure 6. Measurements of flame heights for 19 toluene+methane+hydrogen spray flames as a function of heat release rate.

of an imaginary sphere with radius equal to H_f /2 to obtain the total energy radiated to the surroundings. This estimate divided by the nominal heat release rate for the jet fire based on an assumption of complete combustion yielded an estimate of the radiative heat loss fraction. The results of the single point technique were checked for 5 different flames out of the 19 by completing radial and axial scans of the heat flux to find the actual total energy radiated to the surroundings. In each case, the estimate based on the single point measurement was within 10% of the data based on the full scans. Thus additional support for the single point radiant fraction measurement technique was obtained. This technique proved to be very convenient for completing the X_R measurements for the 19 flames and is highly recommended for future use.

The X_R data for the 19 flames are plotted as a function of the heat release rate in Fig. 7. These measurements show some very interesting trends. For the lowest MLR, the radiant loss fractions are highest for the higher HLR. The X_R for these flames increase from 32% at a heat release rate of 10 kW to approximately 40% at a heat release rate of 25 kW. This result is completely opposite the conventional observations in gas fired jet flames for which the X_R remain independent of firing rate in a range of firing rates and then decrease with further increase. For intermediate MLRs, the X_R do remain relatively constant with increasing heat release rates. For the highest MLR studied, the X_R decrease with increasing heat release rate. The flames with the highest MLR (25%) and higher HLR (13%) show X_R values of approximately 10% which are lower than buoyant methane air flames studied in the past. Thus the present spray flame configuration y lead to a substantial decrease in X_R with approximately 40% gaseous fuels added to the aromatic toluene. Previous work by Skinner and Gore (1992) with acetylene+methane mixture flames showed that the radiative fractions for a gaseous sooty fuel were not reduced with the addition of methane by a significant amount. Thus the observed reduction appears to be characteristic of the spray flames and needs to be examined further. The filled symbols in Fig. 7 show the data for the flames with lower HLR. The sooting tendency increases with reduction in the HLR hence higher values of X_R would be expected based on intuition. However, the coupling between soot formation, radiative heat loss, flame temperature, and self absorption of emitted radiation by soot particles in the colder regions of the flame leads to the present result.

Figure 8 shows measurements of average emission temperatures as a function of distance from the burner exit obtained using two wavelength emission pyrometry for 5 flames selected for detailed study. The flames represent a factor of 2 change in heat release rate, a factor of five change in MLR at a fixed heat release rate and a fixed HLR, and a factor of 2.6 change in the HLR at a fixed heat release rate and a fixed MLR. Measurements of average transmittance as a function of axial distance based on extinction of a He-Ne laser beam at 632 nm wavelength are also shown in Fig. 8.

The emission temperature instruments records a temperature only if soot particles with a sufficient volume fraction (greater than 0.1 PPM) at temperatures above 1100 K are present along the diametric path. If these conditions are not satisfied the temperature is automatically set to 300 K. Thus the present instrument is not capable of measuring temperatures of nonluminous flames. For the MLR =25% flame (square symbols in Fig. 8), soot formation occurs only intermittently at locations near the injector exit as shown by the near unity transmittance in the bottom part of the Figure. Thus the apparent average temperature is very low (approximately 500 K). As the distance

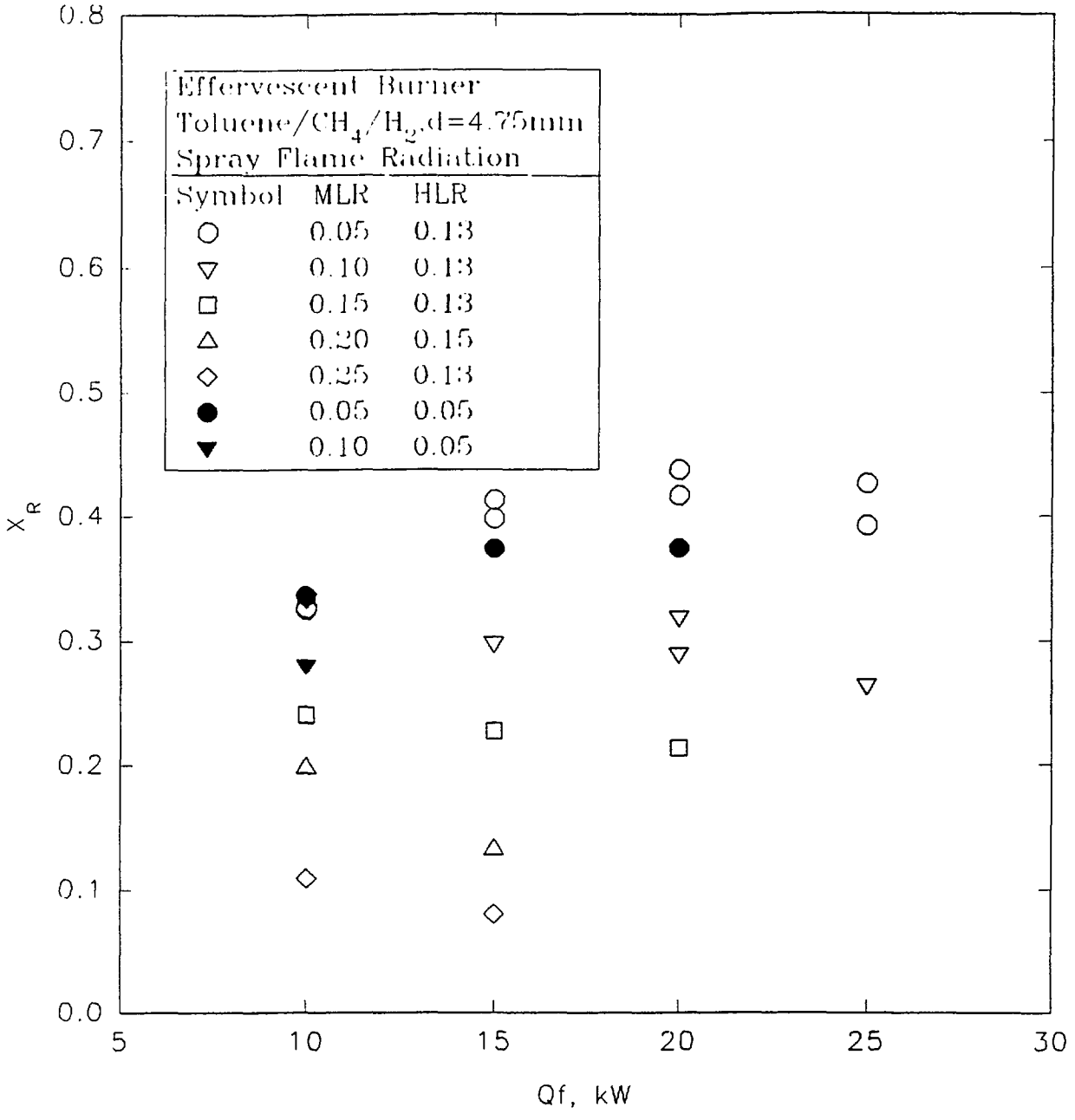

Figure 7. Measurements of radiative loss fractions for 19 toluene+methane+hydrogen spray flames as a function of heat release rate.

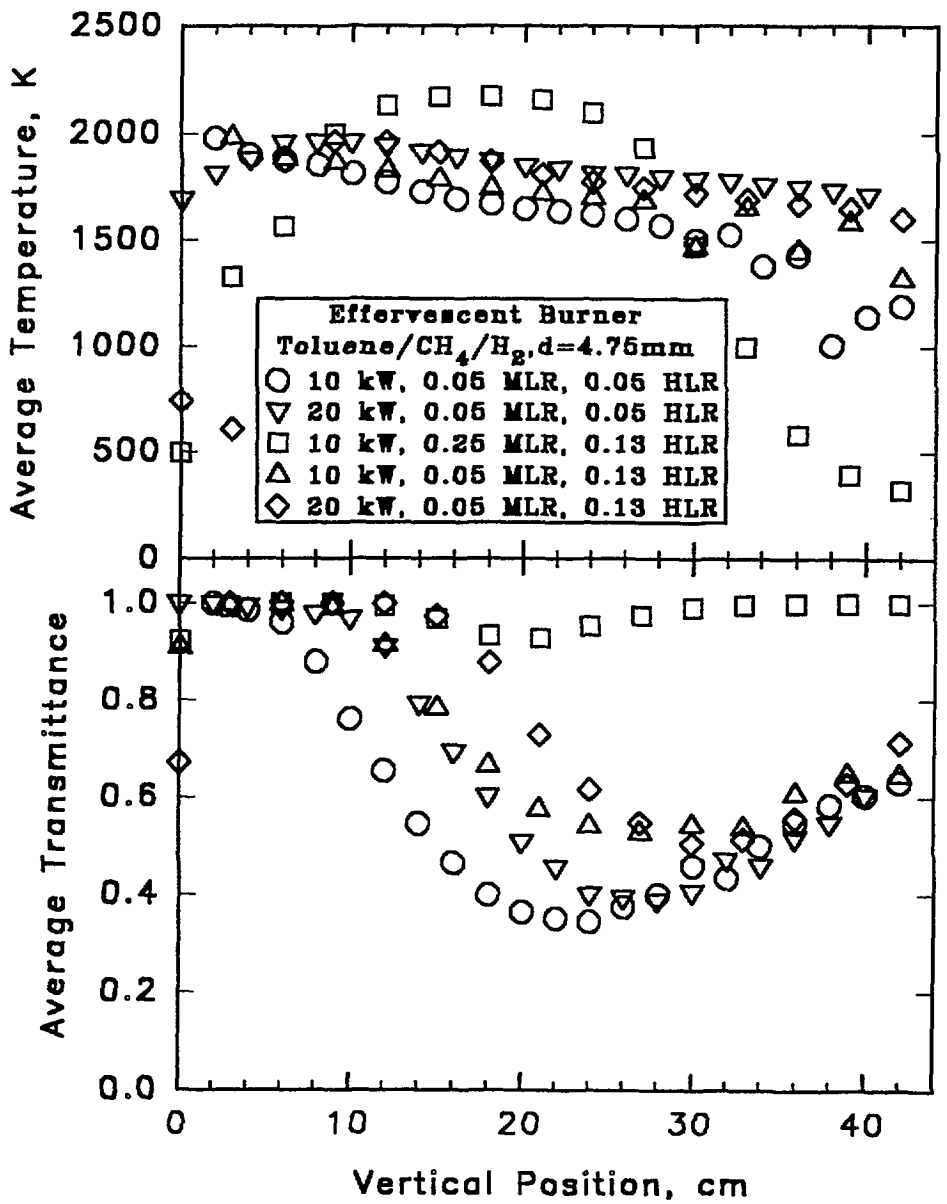

Figure 8. Measurements of average path integrated emission temperatures and transmittance for 5 representative toluene+methane+hydrogen flames.

from the burner exit increases, the average transmittance decreases to approximately 0.95 and the average emission temperature for this flame increases to approximately 2200 K at a distance of 20 cm above the injector. This is the highest detected emission temperature amongst all the flames. As distance from the burner exit is increased further, the soot particles in the MLR=25% undergo significant oxidation and the observed average temperature decreases continuously to 500 K at 40 cm due to lack of emission signal. This is confirmed by the unity transmittance at positions above 30 cm. The radiative loss fraction for this flame is only 10% in spite of the high temperatures due to the high transmittance caused by lack of emitting soot particles.

The MLR for the remaining four flames selected for a detailed study is 5%. All of these flames form significant amount of soot particles. In fact as indicated by the relatively low transmittance at relatively high positions in the flame, soot is emitted to the surroundings by these flames. The 20 kW flame with higher HLR shows significant amount of soot particles only at a height of 5 cm from the burner exit where the temperature reaches approximately 2000 K. Since the measured temperatures are path integrated, these change only due to the effects of radiative heat loss at axial locations before the visible flame tip as long as soot particles in detectable quantities exist in the flame. The measurements of temperature and transmittance for the flames with 10 kW heat release and MLR =5% with two different HLRs (5% and 13%) allow a consideration of the unexpected trend in radiative heat loss fraction with changes in HLR observed in the present measurements. The 10 kW flame with a 5% HLR has the lowest transmittance over the distance shown in Fig. 8. The peak emission temperature in this flame is 1900 K near the injector exit and decreases due to radiative cooling to the 1400 K to 1200 K range between axial distance of 30 to 40 cm. The low transmittance and visual observations also indicate emission of soot by this flame into fuel lean regions and into the surroundings. Therefore, absorption of radiation emitted by the hot region by the surrounding cold soot particles is likely. These factors combine to result in a radiative loss fraction of approximately 32 % for this flame. If the HLR is increased to 13 %, the sooting tendency decreases as shown by the higher value of the measured transmittance in Fig. 8 (triangle symbols). The emission temperature increases by approximately 50 K leading to a compensation for the increased transmittance. Thus the flame radiates almost 32 % of its energy to the surroundings similar to the low HLR flame with higher soot loading. The emission temperatures of the flames that do not form significant amounts of soot near the burner exit and therefore do not undergo radiative cooling remain higher for a longer distance leading to a longer visible flame length as seen from a combination of Figs. 6 and 8. The flames with lower HLR form larger amounts of soot near the burner exit and undergo radiative cooling and hence appear shorter in terms of luminous flame length. The region downstream of the flame tip shows copious amount of smoke emission to the exhaust. The flames with very high MLR appear shorter because all of the soot particles are oxidized within the flame leading to a clear nonluminous zone downstream of the luminous flame tip.

The above data indicate that radiative cooling as well as soot oxidation processes have a significant influence on the apparent luminous flame height. Part of the changes observed in Fig. 6 with heat release rate are also due to the changes in the tendency to form soot in early parts of the flame. Therefore, local soot volume fractions in the flames are discussed in more detail in Chapters 2 and 3.

References (Chapter 1)

Dutta P., Gore J. P., Sivathanu Y. R., and Sojka P. E., 1994, Global Properties of High Liquid Loading Turbulent Crude Oil +Methane/Air Spray Flames," Combustion and Flame, 97:251-260.

Evans D. D., 1991, Personal Communication.

Gore J. P. and Evans D. D., 1991, "Technology Assessment and Research Program of the Offshore Mineral Operations," OCS Study MMS 91-0057, J. B. Gregory, C. E. Smith, and E. J. Tennyson, Eds., United States Department of Interior, Washington D.C.

Hustad H. and Sonju O. K., 1986, "Radiation and Size Scaling of Large Gas and Gas/Oil Diffusion Flames," Dynamics of Reactive Systems Part I: Flames and Configurations, J. R. Bowen and R. I. Soloukhin, Eds., Vol. 105, Progress in Astronautics and Aeronautics Series, AIAA, New York, pp. 365-387.

Sivathanu Y. R., Gore J. P. and Dolinar J., 1991, " Transient Scalar Properties of Strongly Radiating Jet Flames," Combust. Sci. and Tech., Vol. 76, pp. 45-66.

Sivathanu Y. R. and Gore J. P., 1993, "Total Radiative Heat Loss in Jet Flames from Single Point Radiative Flux Measurements," Comb. Flame, Vol. 94, pp. 265-270.

Sivathanu Y. R. and Gore J. P., 1993, "A Tomographic Method for Reconstruction of Local Probability Density Functions," Journal of Quantitative Spectroscopy and Radiative Transfer, Vol. 50, No. 5, pp. 483-492.

Swan W. E., Dutta P., Gore J. P. and Sojka P. E., 1994, "Evaporation Length Measurements in High-Liquid Loading Turbulent Crude-Oil +Methane/Air Jet Diffusion Flames," Proceedings of the Central States Section of the Combustion Institute, Madison, Wisconsin.

Zhou X. C. and Gore J. P., 1994, "Particle Imaging Velocimetry of Flow Field Induced by a Small Toluene Pool Fire," ASME Winter Annual Meeting, Chicago, accepted, Combustion and Flame, submitted.

CHAPTER 2 : MEASUREMENTS OF PATH INTEGRATED TRANSMITTANCES

Measurements of probability density functions (PDFs) of transmittance for several radial chords at three different axial stations for the five representative toluene/methane/hydrogen - air flames selected for detailed study were completed. The mean transmittance and emission temperature measurements involving axial profiles for diametric paths within these flames are discussed in Chapter 1. Based on the interesting features revealed by these data, measurements of the transmittance statistics for radial chord-like paths were undertaken. These data can yield the statistics of the local transmittances up on deconvolution. In view of turbulence-radiation

interactions and the apparent effects of radiation on spray flame heights, local soot volume fraction data are of interest.

The operating conditions for the five flames, selected for local soot statistics study, are summarized in the following Table:

No.	Q, kW	MLR	HLR	H_f, cm	X_R %
1	10	0.05	0.05	43	34
2	20	0.05	0.05	55	37
3	10	0.25	0.13	33	11
4	10	0.05	0.13	45	33
5	20	0.05	0.13	59	44

As seen from the Table, the selection of the operating conditions allows an examination of: the effects of heat release rate with fixed MLR and HLR (flames 1 and 2; 4 and 5), the effect of changes in HLR (flames 1 and 4; 2 and 5), the effects of changes in MLR (flames 3 and 4) on flame height and radiative loss fraction. It can be seen that increase in heat release rate leads to an increase in flame height and radiative loss fractions with fixed MLR and HLR consistent with earlier observations with spray flames. This effect is very significant in the present range of operating conditions. Increase in HLR leads to an increase in flame height and in one case leads to increase in radiative loss fraction and in the other case a constant heat loss fraction. The addition of H_2 reduces soot formation. However, due to reduced local radiative heat loss, the temperature levels are higher leading to identical overall radiative heat loss fractions. This effect is very interesting. Finally, increase in MLR leads to significant reduction in flame height and radiative loss fractions. In fact, flame number 3 has a radiative loss fraction of 11 % which is comparable to high momentum methane jet flames.

Measurements of path integrated transmittances in the visible (632.8 nm) and effective emission temperatures for diametric paths in the five flames showed that MLR has a strong influence on soot formation. The data also showed that the radiative cooling in the flame with 10 kW heat release rate with 5% MLR and 5% HLR occurred faster than that in the 20 kW flame with identical MLR and HLR. This effect resulted from higher residence time for soot formation and increased radiative cooling due to both higher soot volume fractions and greater residence time in the 10 kW flame. The flame with 10 kW heat release rate and MLR=15% had very little soot formation and showed relatively low radiative heat loss fractions. The reason appears to be a significant decrease in residence time due to the high momentum methane jet. However, details of the processes that suppress soot formation in this configuration are unknown. In order to gain a better understanding of the local soot processes, path integrated measurements of probability density functions (PDFs) of transmittances at various radial locations at three different heights were conducted in the five flames. These data will be used to obtain PDFs of local transmittances and soot volume fractions using a novel technique developed at Purdue.

Figure 1 shows the PDFs of transmittance for 22 radial positions within the 10 kW, MLR =5 %, HLR =5% flame at three different heights. Relatively high transmittance values are observed for the $x = 0.25H_f$ position indicating that significant distance (residence time) is needed for the soot formation process to initiate in the spray flames. At the two higher positions, the lowest transmittance values and the shape of the PDF curves are similar. At all radial positions,

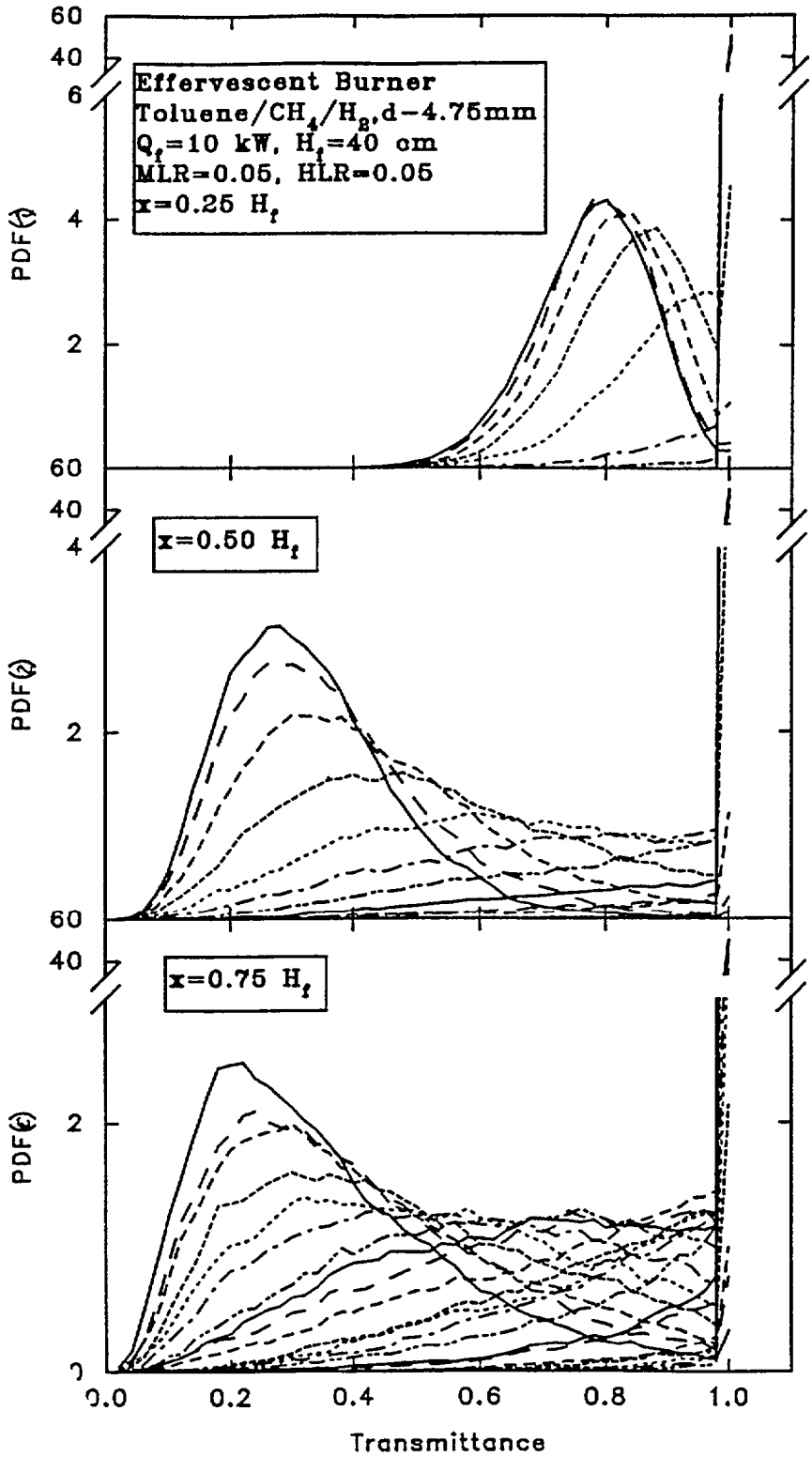

Figure 1. Transmittance for Chordlike Paths for 10 kW Toluene/Methane/Hydrogen Flame with MLR=5% and HLR=5%.

the soot appears in an intermittent fashion as indicated by a peak in the PDF curve at a transmittance value close to unity.

The PDFs of transmittance at three axial positions in the 20 kW spray flame with MLR = 5% and HLR = 5% for three axial positions at several radial locations are shown in Fig. 2. These data show that due to the relatively higher momentum of the 20 kW fire, the transmittance values at the $x = 0.25H_f$ position are even higher than those for the 10 kW flame. The peaks in the PDF for lower transmittance values observed for the 10 kW flame are not seen at the lowest position. The behavior at the two higher positions is qualitatively similar to that for the 10 kW flame but the magnitudes of the transmittance value are higher. Thus it appears than the sooting tendency is decreasing with increasing heat release rate. Similar to the 10 kW flame, the spike in the PDF at unity transmittance is observed once again.

The effect of higher hydrogen flow rate on the soot volume fractions is seen in Fig. 3 where PDFs of transmittance are plotted for three axial positions for the 10 kW flame with MLR = 5% and HLR =13 %. The Fig. shows that the addition of excess pilot flame hydrogen delays the formation of soot as indicated by the lower probabilities at lower transmittances. Soot streaks indicated by the peak in the PDF at a lower transmittance value are not observed to form at the lowest position. The value of the transmittance at which the peak PDF occurs has shifted from 0.25 to 0.4 with the increase in hydrogen flow at $x = 0.5\ H_f$. The PDFs at $x = 0.75\ H_f$ flame show very interesting behavior. The soot streaks indicated by a PDF peak at a low transmittance value have disappeared perhaps due to the enhanced oxidation and mixing caused by the higher temperatures resulting from the hydrogen pilot. At all three locations, a spike in the PDF at unity transmittance is observed indicating that soot containing gases are intermixed with gases with no soot in an intermittent manner.

Figure 4 shows the effect of additional hydrogen flow rate on the PDF of transmittance for the 20 kW flame. The onset of soot formation is certainly delayed based on the PDFs at $x = 0.25\ H_f$. The soot formation process does commence and reach levels sufficient to yield transmittance values close to those observed in the 10 kW flame. The transmittance values at $x = 0.75\ H_f$ show that the oxidation process in the 20 kW flames appears to be some what slower than that observed in the 10 kW flame.

The PDFs of transmittance at three different heights for various radial positions in the 10 kW flames with MLR=25 % and HLR =13% are plotted in Fig. 5. The transmittance values are very high indicating that the soot formation process in these flames is suppressed probably due to the high exit momentum ratio of the methane jet. The PDFs at all three positions do not show a separate peak at a lower transmittance value indicating that soot streaks are not formed in these flames.

The reduction in soot formation rate caused by the higher methane flow rate is very interesting but has not been understood yet. Local soot volume fraction statistics are expected to provide further insight into this behavior. In Chapter 3, the local soot volume fraction statistics for the conditions of the transmittance measurements discussed above are presented.

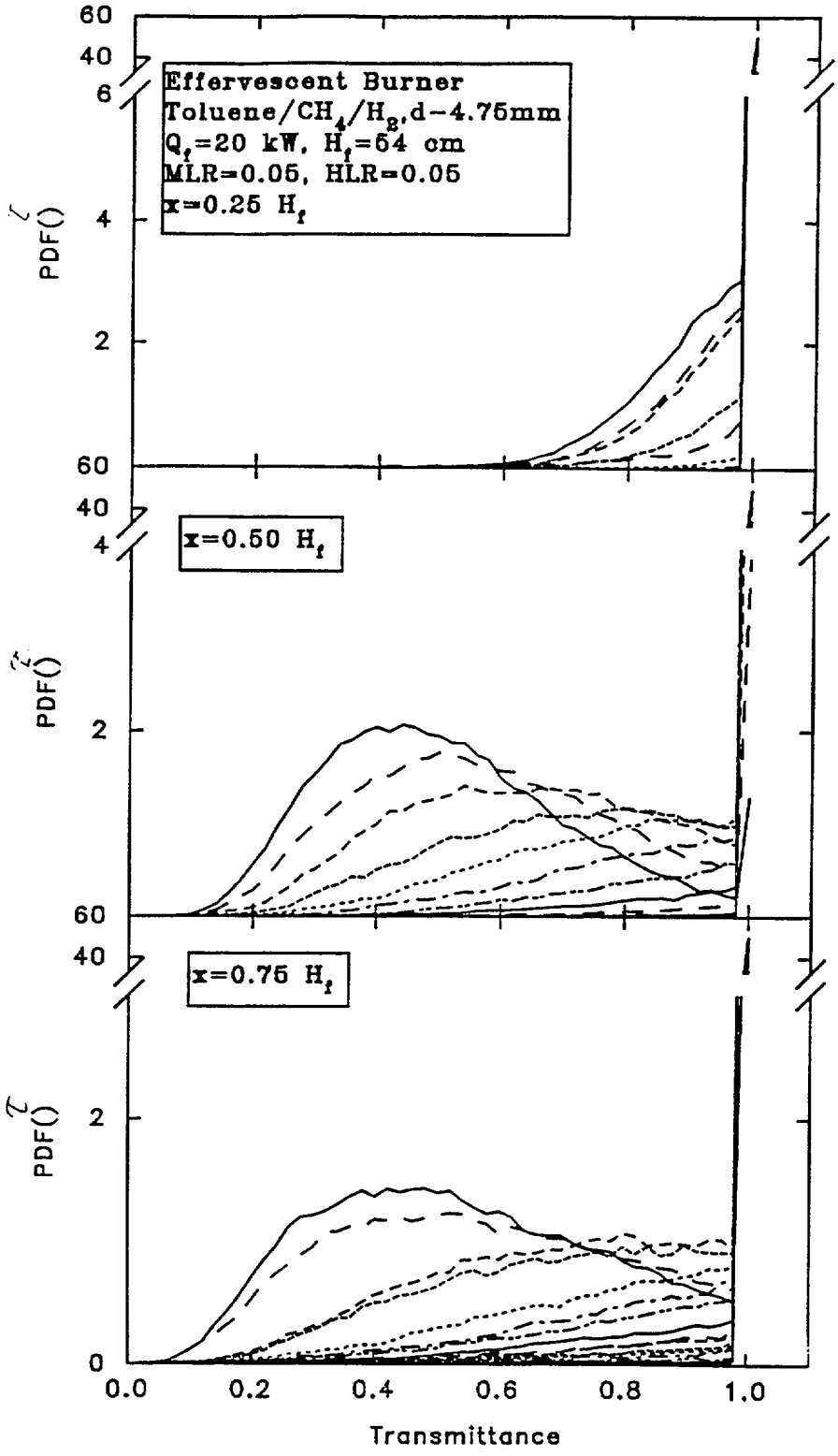

Figure 2. Transmittance for Chordlike Paths for 20 kW Toluene/Methane/Hydrogen Flame with MLR=5% and HLR=5%.

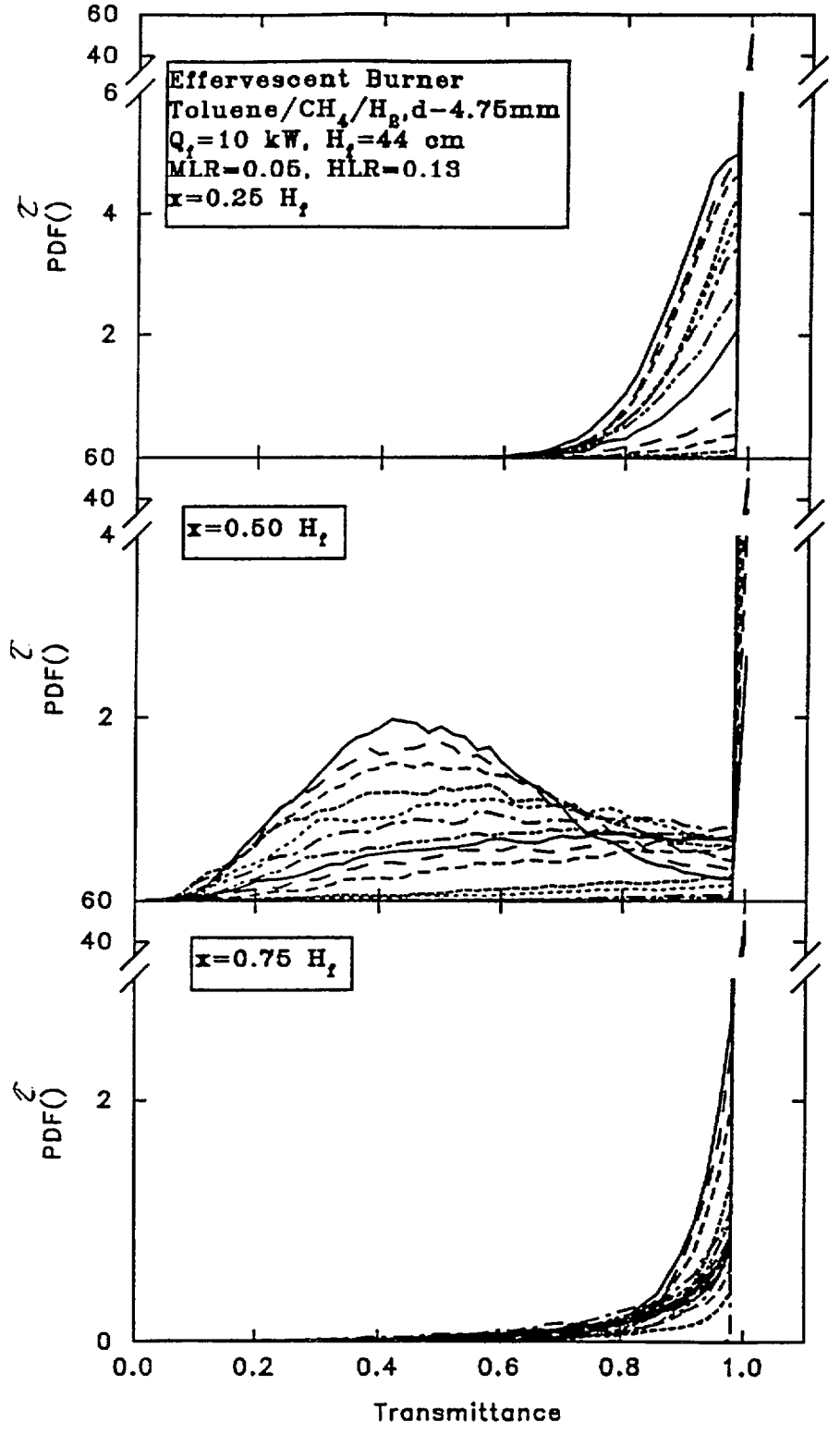

Figure 3. Transmittance for Chordlike Paths for 10 kW Toluene/Methane/Hydrogen Flame with MLR=5% and HLR=13%.

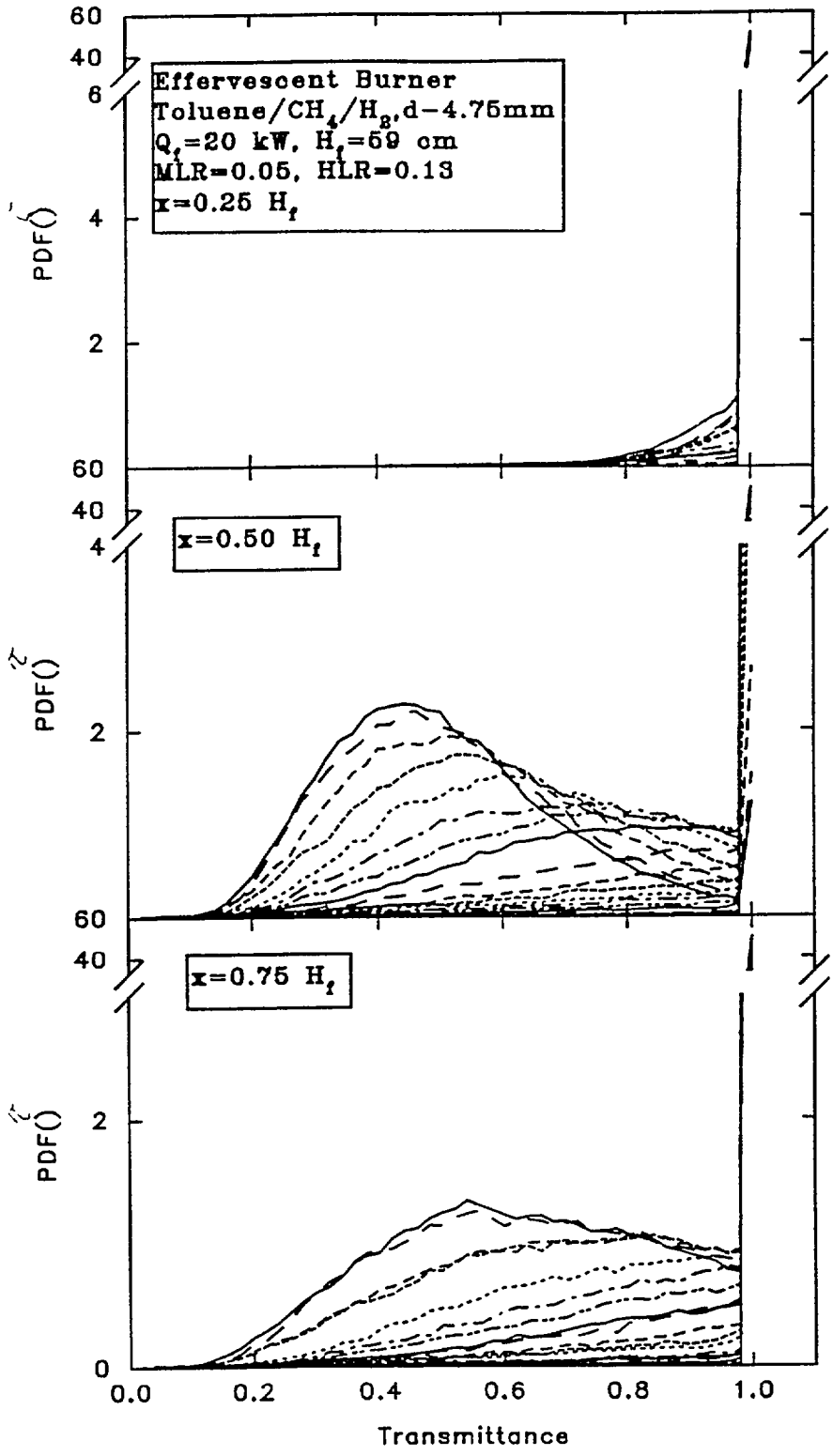

Figure 4. Transmittance for Chordlike Paths for 20 kW Toluene/Methane/Hydrogen Flame with MLR=5% and HLR=13%.

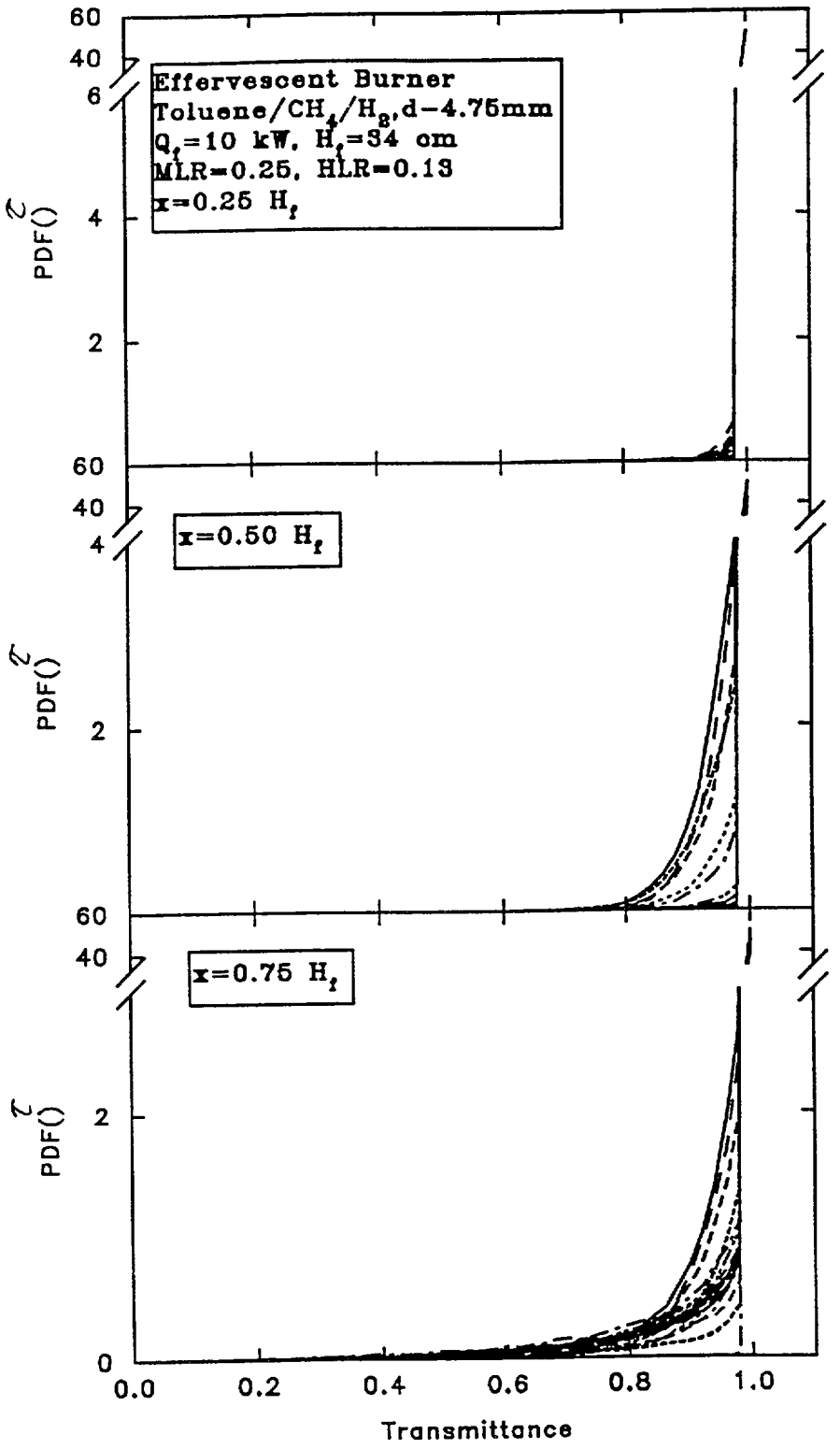

Figure 5. Transmittance for Chordlike Paths for 10 kW Toluene/Methane/Hydrogen Flame with MLR=25% and HLR=13%.

CHAPTER 3 LOCAL STATISTICS OF SOOT VOLUME FRACTIONS

Introduction

Accidental rupture of liquid storage tanks, puncture of pipelines, and oil well blowout fires may cause hazardous high liquid loading spray fires [1]. Material exiting the accidental leaks has high liquid loading with small vapor fractions. The vapor can cause atomization and vaporization of liquid fuel leading to spray flame stabilization. A full understanding of these fires will allow industrial designers to minimize the potential hazard to personnel. Dutta et.al. [2] found that these flames have not been studied extensively in the literature, but can be very important for fire safety issues. An example of these fires can be found in the work of Evans et.al. [1] who asses the heat release rate of the crude oil well fires in Kuwait using flame height and thermal radiation measurements. The mass of lost the crude oil was sought from the measured global properties of radiative heat loss fraction and visible flame length. Enhanced understanding of spray jet flames will contribute to the assessment of economic losses and enhancement of fire safety.

The visible flame length is strongly influenced by its sooting tendency. The flame is visible primarily due to the glowing soot particles. As the concentration and temperature of the soot particles increase, the visible flame length is expected to increase. Soot concentration and temperature also strongly effect the radiative heat loss which cools the flame and decreases the visible flame length. The objective of the present paper is to report measurements of soot volume fractions and temperatures in high liquid loading spray jet fires and interpret these in terms of the visible flame length and radiative loss fraction data.

Theoretical Background

Following ref. [3], line of sight measurements of monochromatic absorption and two wavelength emission are obtained for chord-like paths at various heights in the flames. The line of sight absorption data are related to an effective soot volume fraction [4]. However, following ref. [5], these data can also be used to find local soot volume fractions.

Beer's law gives an expression for absorption soot volume fraction, f_v (ppm), when the soot particle diameters are below the Rayleigh limit.

$$f_v = \frac{-\ln\left(\frac{I_\lambda}{I_{\lambda^o}}\right)\cdot\lambda}{k_\lambda \cdot L} \qquad (1)$$

The argument of the logarithm is the intensity ratio of light that passes through the medium to the incident light. This ratio is the transmittance, t_l. In this expression k_l, given by eqn. (2), is the spectral extinction coefficient which is an optical property of the soot based on its refractive indices.

$$k_\lambda = \frac{36\pi\cdot n\cdot k}{(n^2 - k^2 + 2)^2 + 4\cdot n^2\cdot k^2} \qquad (2)$$

The value of k_l for a He-Ne laser at 632 nm is 4.892 based on a soot refractive index of 1.57-0.56j. These expressions allow the measurement of soot volume fraction knowing wavelength, geometry, spectral absorption coefficient, and transmittance. The wavelength is specified by using a laser, the geometry is determined by the experimental apparatus, the spectral absorption coefficient is calculated using eqn. (2), and the transmittance is obtained experimentally. The emission intensity leaving a volume of soot is given by:

$$I_{\lambda e}=\frac{\left(1-e^{\frac{-k_\lambda \cdot f_v \cdot L}{\lambda}}\right)\cdot 2\cdot h\cdot c^2}{\lambda^5\cdot\left(e^{\frac{h\cdot c}{\lambda\cdot k_b\cdot T}}-1\right)} \qquad (3)$$

k_l is the spectral absorption coefficient, L is the path length, f_v is the effective soot volume fraction based on emission, h is Planck's constant, k_b is the Boltzmann's constant, and c is the speed light in vacuum. This expression can be expanded using a two term Taylor series. Intensity is a function of wavelength for a source at a fixed temperature. The soot volume fraction and path length drop out of the expression if a ratio of these intensities is taken using the expansion. The result gives the ratio of intensities.

$$\frac{I_{\lambda 1}}{I_{\lambda 2}}=\frac{k_{\lambda 1}\cdot\lambda_2\cdot\lambda_2^5}{k_{\lambda 2}\cdot\lambda_1\cdot\lambda_1^5}\cdot e^{\frac{h\cdot c}{k_b\cdot T}\cdot\left(\frac{1}{\lambda_2}-\frac{1}{\lambda_1}\right)} \qquad (4)$$

The two wavelengths used in this study are: 900 nm and 1000 nm, where the soot spectral extinction coefficients are k_{900}=5.288 and k_{1000}=5.473. The intensities are measured experimentally and the expression is solved for the effective temperature T of the path L.

Line of sight absorption measurements are used to investigate soot volume fraction properties in the flames. These data are deconvoluted to obtain local properties. The flame is taken to consist of axisymmetric rings, with each ring having an effective soot volume fraction. As the laser passes through the flame, each ring makes a contribution to the light absorbed by the path. Local properties can be obtained using a deconvolution scheme. Path integrated values for temperature and local values for soot volume fractions obtained using a novel deconvolution procedure based on probability density functions (PDF) are reported. Local values of temperatures will be obtained in future studies.

Local properties give an enhanced understanding for the highly non-linear processes like radiative heat transfer and chemical kinetics. Deconvolution is complicated by the turbulent nature of the jet spray flames which is partly described by the PDF. Each path integrated PDF must be deconvoluted ring by ring to gain a knowledge of the local properties. The deconvolution method is called the Abel integral method and is commonly referred to as "onion-peeling." Each ring has a characteristic PDF for transmittance. Absorption measurements over a path consisting of segments of two rings yields the product of the transmittances, $t_T=t_1t_2$. The probability for a specific value of transmittance in the total path is related to the probability of each realization of the transmittance in the two rings. The transmittance is also related to the geometry of the rings. Each PDF is discretized and each bin is processed in relation to all other bins of the other discrete probability density functions [5]. The outer most chord in the flame

makes the first PDF. The second chord crosses two rings from which knowledge of the total path integrated PDF and the PDF for the outer ring can be used to solve for the PDF over the inner ring. Thus PDF deconvolution works its way into the center of the flame to give local PDFs for each ring [5]. The local soot volume fraction averages are found from the local PDF.

The average transmittance for each chord-like path can be used to obtain an estimate of the local average soot volume fraction. However, this procedure results in the neglect of the effects of turbulent fluctuations on transmittance. In the present work, the errors caused by such a neglect are shown quantitatively.

Experimental Methods

High liquid loading spray jet flames with gas to liquid ratios between 0.05 and 0.25 are stabilized over an effervescent atomizer burner [2]. Toluene (C_7H_8) is used as the liquid fuel. Methane (CH_4) is used as the atomizing gas. A small hydrogen (H_2) pilot ring flame stabilizes the spray flame. The two phase flow from the atomizer is best characterized using the total combined heat release rate (Q_f) computed from the nominal heating values of 39,912 kJ/kg for toluene, 50,144 kJ/kg for methane, and 109,921 kJ/kg for hydrogen. At each heat release rate, variation of the methane to liquid mass ratio (MLR) and Hydrogen to liquid mass ratio (HLR) resulted in 19 test conditions. Five of these conditions were selected, as shown in Table 1, for measurements of soot volume fractions. The operating conditions ranged in heat release rate from 10 kW to 25 kW, MLR varying from 5% to 25% and HLR varying from 5% to 13%. This test matrix allowed a study of the influence of each parameter. Each of the five flames were studied at three representative axial locations selected to be 1/4, 1/2 and 3/4 of the visible flame length, H_f.

The experimental arrangement for the absorption and emission measurements is shown schematically in Fig. 1.

Absorption measurements require a known light intensity to be directed through the flame and detection of the resulting intensity after the flame. This is accomplished using a 5 mW He-Ne laser, a beam splitter, and laser power meters (photo diode) on either side of the flame. To minimize noise, the laser beam was chopped at 2000 Hz and the output signals were passed through a high pass filter, a lock in amplifier, and a low pass filter. A reference measurement is made without the flame to determine the incident intensity.

The temperature is determined using the emitted light intensity from the hot soot. Narrow band filters at 900 nm and 1000 nm wavelength were placed over the two photomultiplier tubes. The output signal was passed through a low pass electronic filter. The photomultiplier tubes were calibrated by sampling their output when exposed to a black body radiation source. A collimating tube was used to define the view of the photomultiplier tubes. It is important to note that the measured temperatures represent an effective average of the hot soot along the radiation

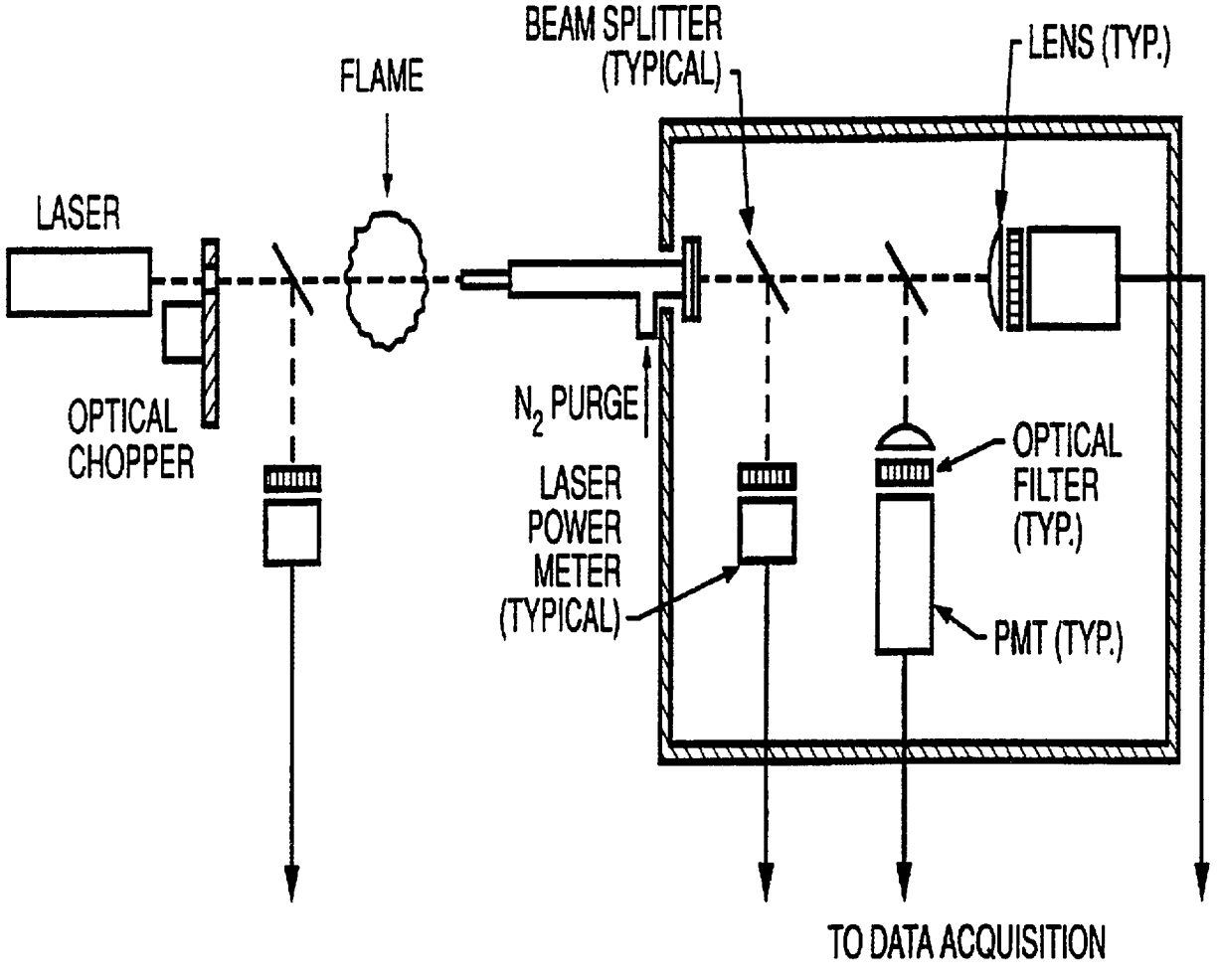

Figure 1: Experimental Setup

path. Any cold soot in the flame and hot gases do not contribute to the emission signals at 900 and 1000 nm. When the emission signal is low the effective temperature is set to 300 K. This procedure introduces severe downward bias in the absence of soot particles.

All the signal voltage output values were sampled by a computer using a four channel A/D board sampling at 1000 Hz. Each measurement lasted 5 seconds so that the turbulent fluctuations of the flame are captured statistically. The burner was mounted on a slide for simple adjustment while the optics remained stationary. The initial position of the burner had the laser pass through the center of the flame and then the burner was radially advanced until the oscilloscope display from the photo multiplier tubes gave no signal indicating that the sooty part of the flame was no longer in the view field.

Table 1: Operation Conditions

Q_f, kW	Toluene, mg/s	MLR, %	HLR, %	H_f, cm	X_R
10	206	5	5	43	.34
10	172	5	13	45	.33
10	147	25	13	33	.11
20	413	5	5	55	.37
20	344	5	13	59	.44

Results and Discussion

Flame Length and Radiative Heat Loss Fraction

The dependence of flame length on soot volume fractions and temperature is sought in this work. Fig. 2 shows that the visible flame length increases as the heat release rate increases. The flame length also increases as the methane to liquid ratio decreases. The radiative heat loss fraction, X_R is the energy leaving the flame by radiative heat transfer normalized by the nominal heat release of the fuel. The radiative heat loss fraction was measured with a radiometer using a single point technique developed in this laboratory[6]. The results were confirmed for some flames by performing a scan of points to form a semiinfinite cylinder. The single point radiation measurements are shown in Fig. 3. For low MLRs, X_R increases and then decreases as the heat release rate is increased. For high MLRs, X_R shows a decreasing trend for all heat release rates. This variety in the X_R variation is caused by coupling between radiative heat loss and flame temperature. The 19 operating conditions demonstrate that there is a wide range of flame lengths and radiative heat loss fractions possible.

Temperature and Soot Volume Fraction Data

The first step in the process of obtaining local properties is sampling the data and creating path integrated PDFs. This was done for the five selected flames and a sample graph for a 10 kW

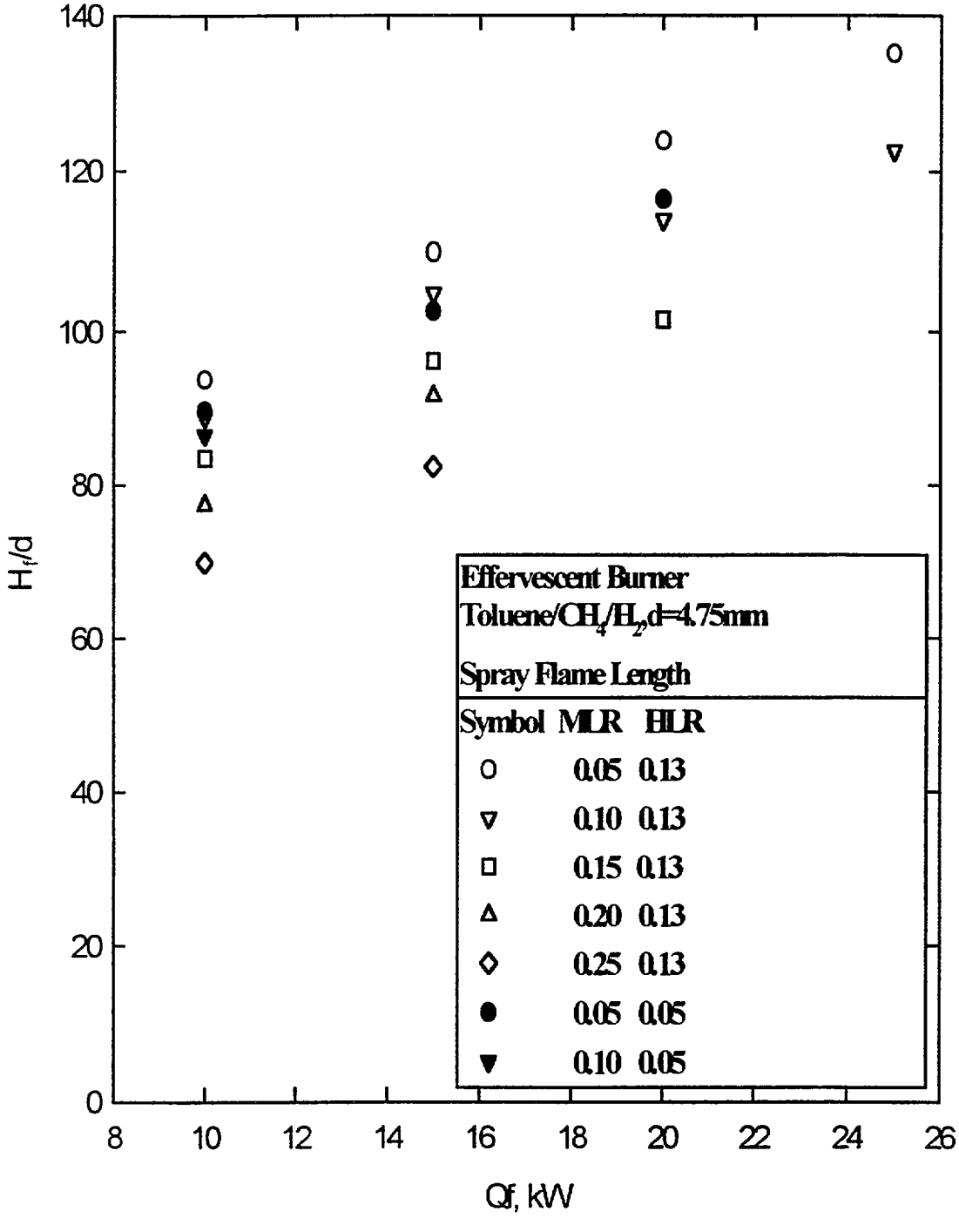

Figure 2: Visible Flame Length

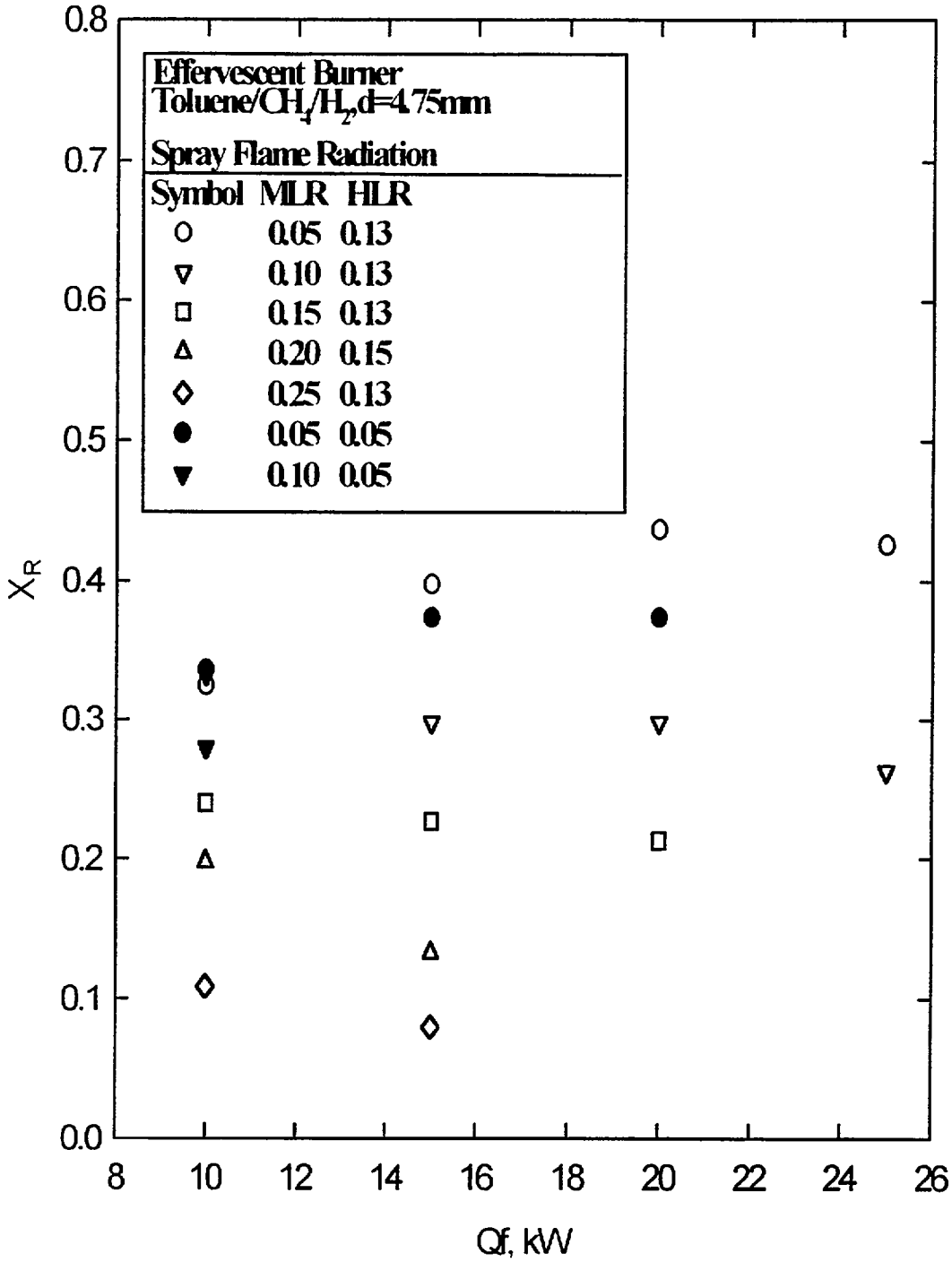

Figure 3: Radiative Fraction of Heat Release

flame at 5% MLR and 5% HLR is shown in Fig 4. Each line in the figure represents one radial position and each box represents a different axial position in the flame. The average values for each radial position in Fig 4 are shown in Fig 5.

The path averaged effective temperature data in Fig. 5 show that temperature is the highest at the diametrical chord where every ring contributes to the path integrated value. The highest temperature in the flame is 1800 K for the 0.25 H_f case. Here the transmittance is 0.8, which is above the values for the other flames at the center. This indicates that the soot volume fractions at this location are lower but the temperatures are higher. At higher positions in the flame, the soot volume fractions increase but temperatures are lower due to radiative cooling. As expected, at higher axial positions in the flame, the transmittance and temperature profiles have a wider radial spread. The temperature of the hot soot was is 1800 K at 0.25 H_f and cooling to 1500 K at 0.75 H_f. The decreasing trend in temperature with increased radial position in Fig. 5 is due to the assigned low values of 300 K being averaged with the measured temperature of the hot soot. Taking the temperature to be constant is only good as a first approximation since the radiation heat loss depends on the temperature in a nonlinear manner.

Local soot volume fraction data are obtained using the deconvolution procedure. Path integrated values are deconvoluted to give local PDFs for transmittance as shown in Fig. 6 for the 10 kW, 5% MLR, 5% HLR flame. Each line represents a radial position and each box represents an axial position.

These PDFs for each radial position in each flame can be processed to obtain graphs of the average values. This allows a simple comparison of large amounts of data. The average soot volume fractions are shown in Fig. 7 for the three 10 kW flames and Fig. 8 for the two 20 kW flames. The average results from the PDF deconvolution method are represented by filled symbols and those obtained from deconvolutions of mean transmittance are shown as open symbols.

Comparing the data at the axial positions for all five flames shows that, the lowest position in the flame has the lowest volume fraction of soot. The highest volume fraction of soot occurs at half of the visible flame length. Soot volume fractions have a peak concentration for the innermost ring and drop off at farther radial positions for the 0.25 H_f flame position. For the 0.75 H_f and 0.50 H_f positions, there is a decrease in soot volume fraction at the center of the flame below the peak value which occurs at a larger radius.

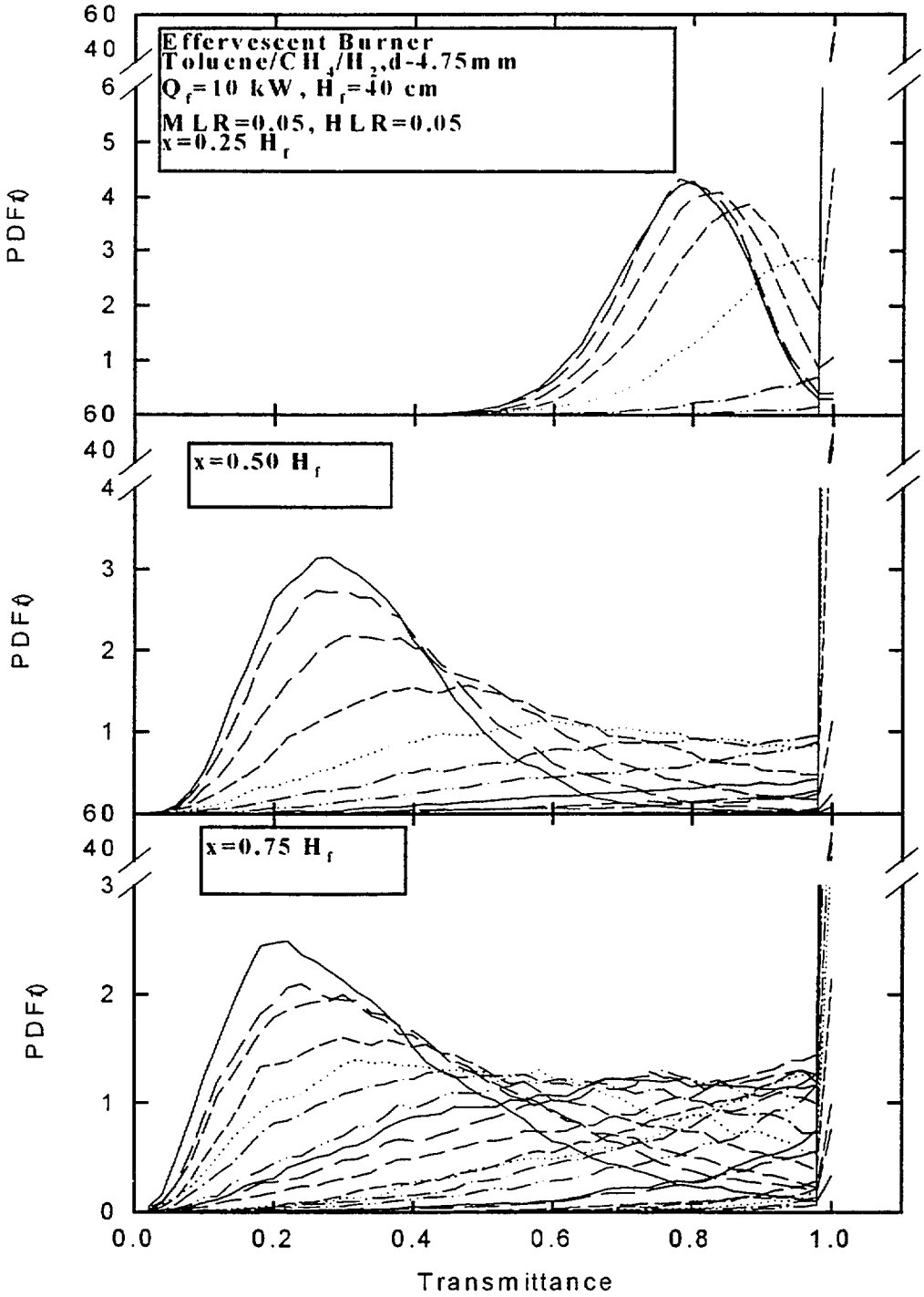

Figure 4 Path integrated PDFs

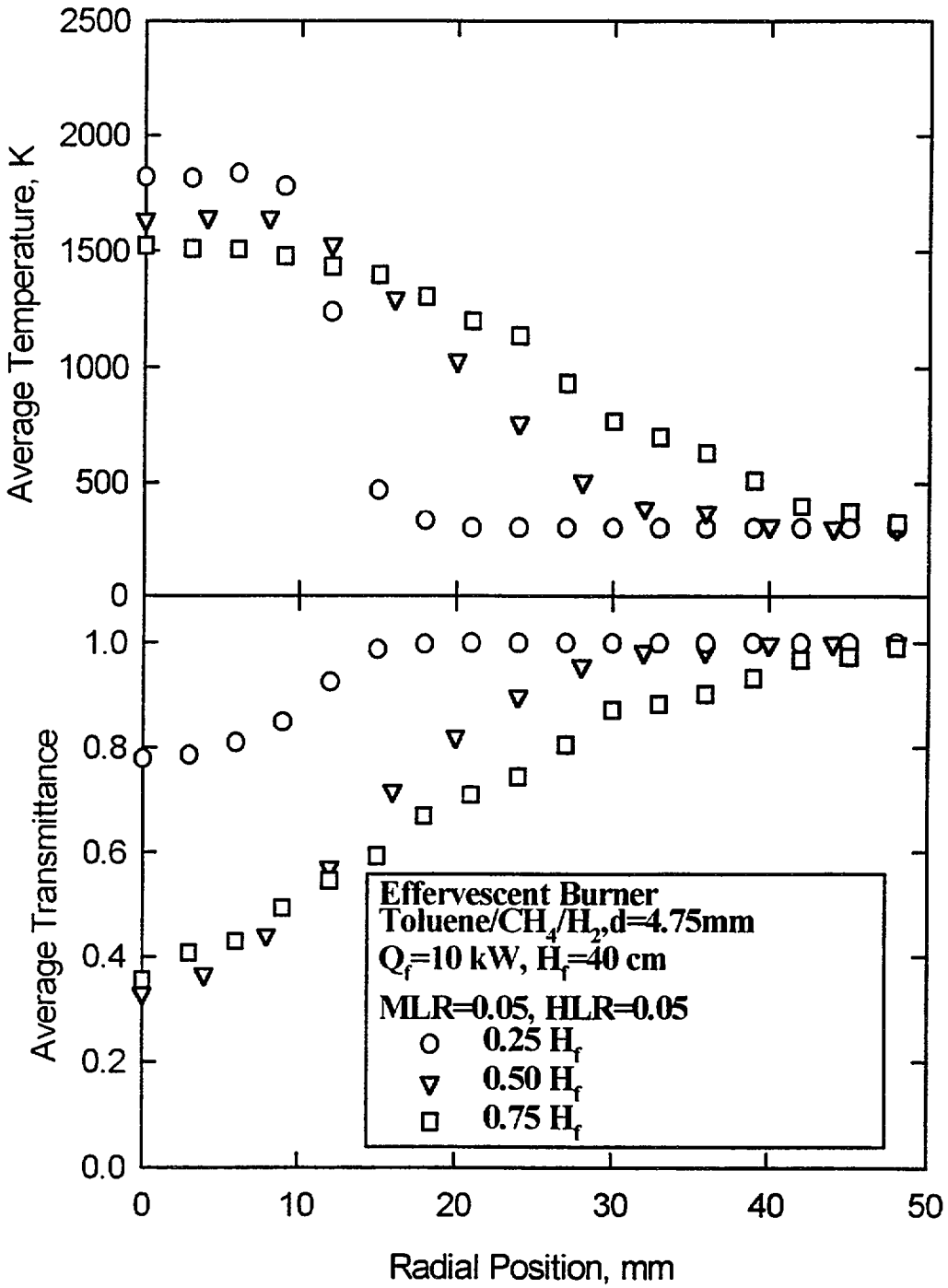

Figure 5: Path Integrated Average Values

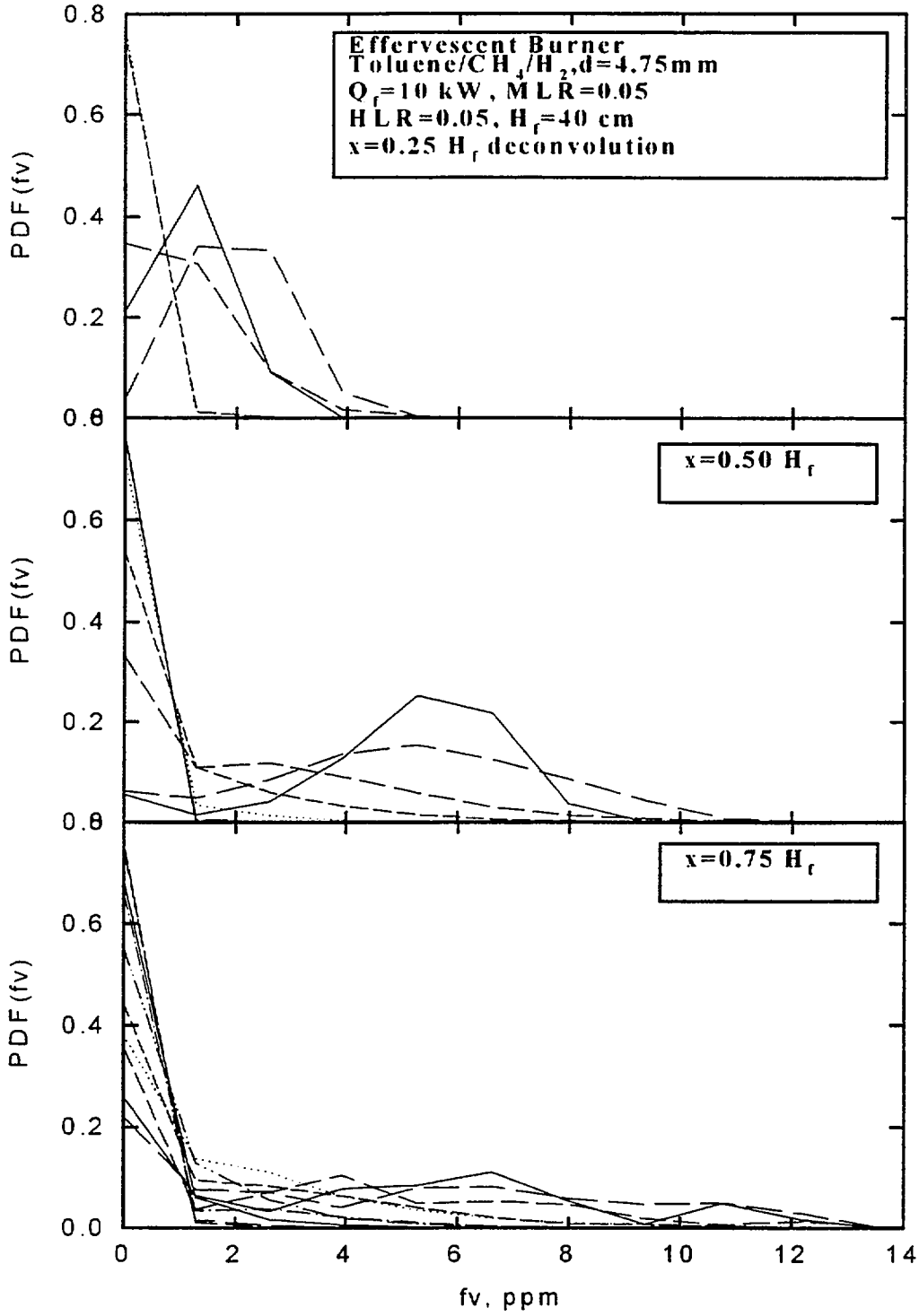

Figure 6: Local PDF of transmittance

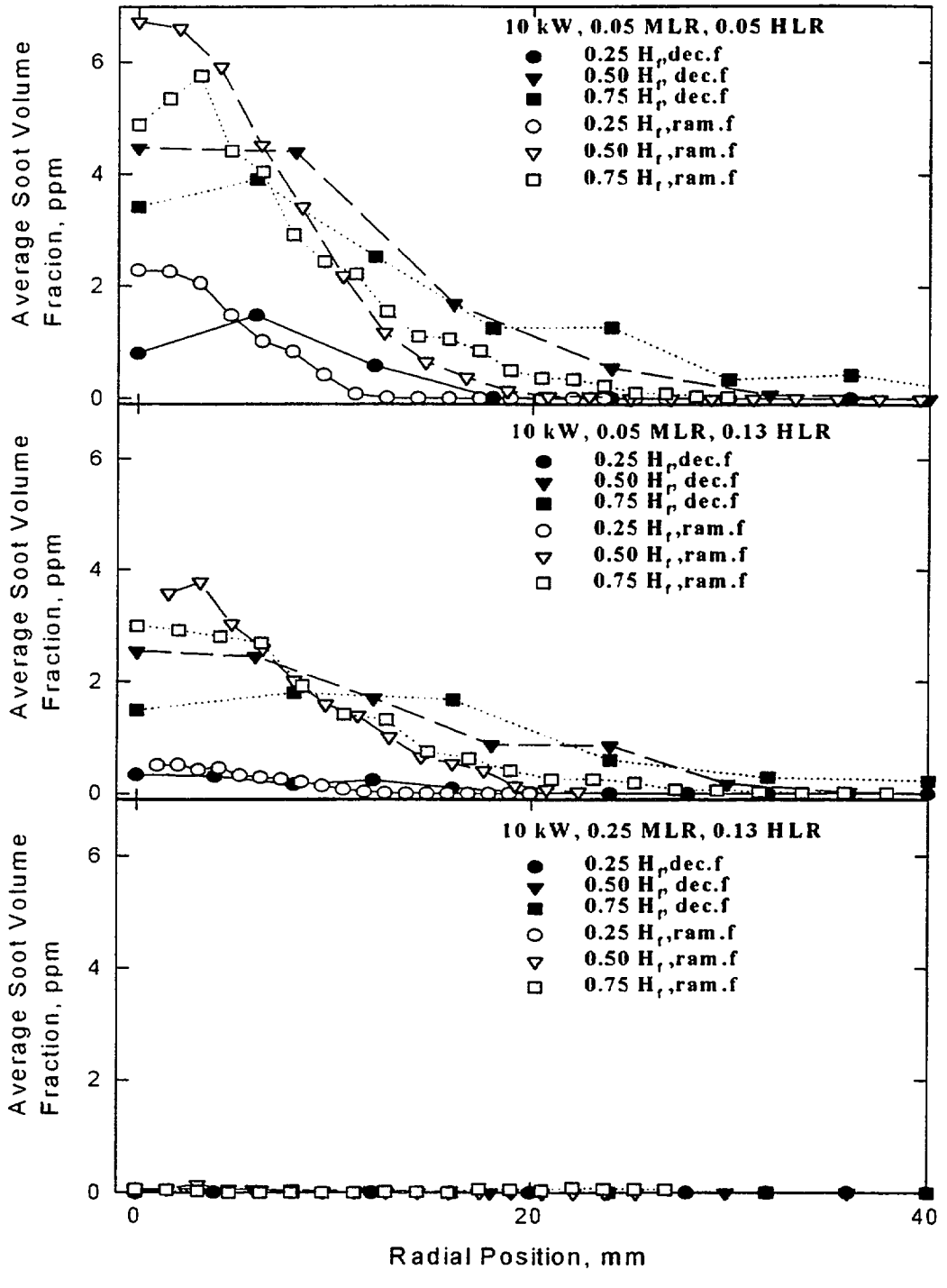

Figure 7: 10 kW Average Soot Volume Fractions

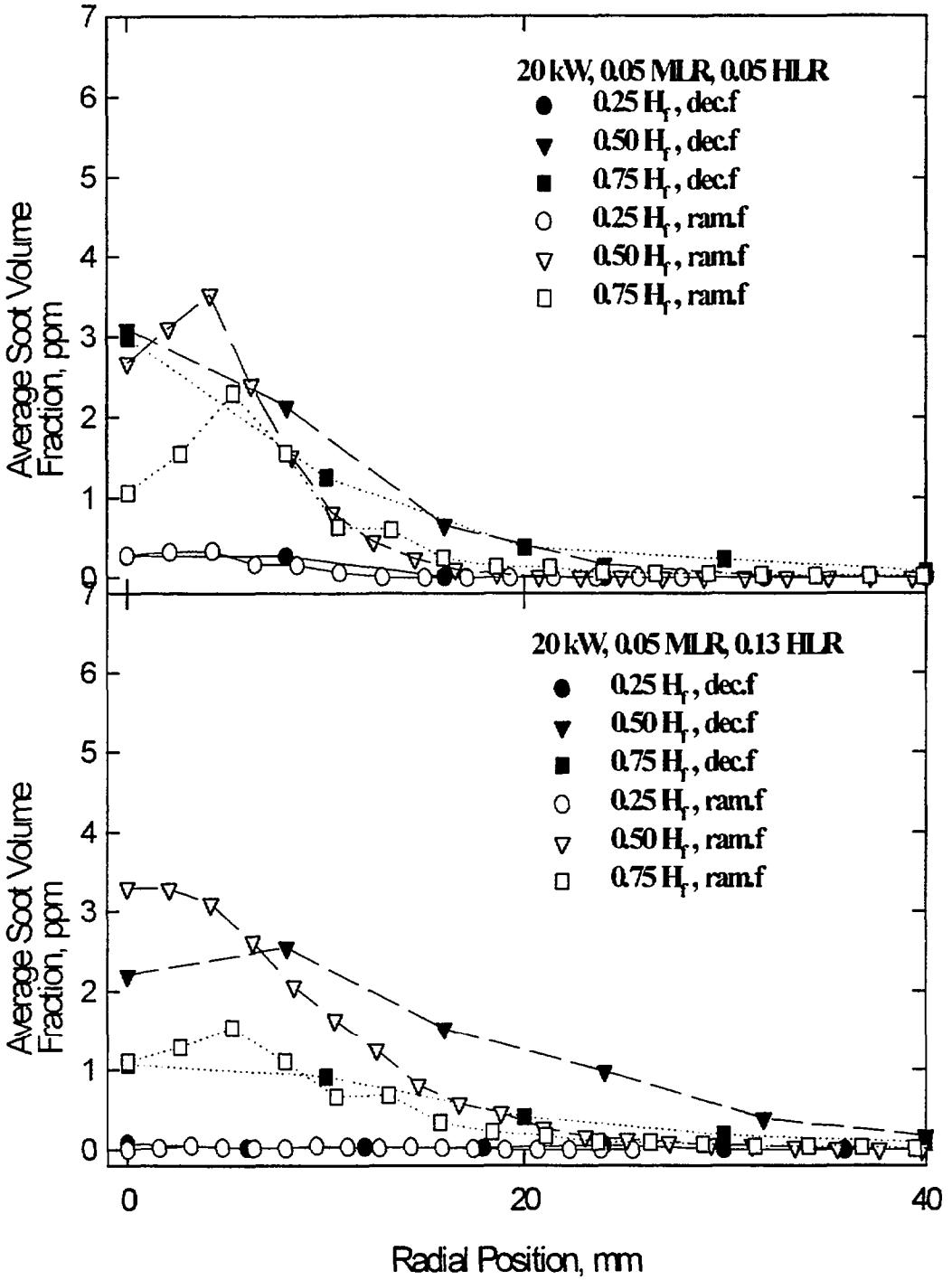

Figure 8: 20 kW Average Soot Volume Fractions

Differences in the trends for the PDF deconvolution based data are primarily in the numerical values of soot volume fraction. The flame with the highest f_v is the one with 10 kW heat release and , 5% MLR, 5% HLR. This flame also shows little decrease in f_v moving from 0.50 H_f to 0.75 H_f. The high f_v makes the flame visible for the longest length among the seven 10 kW flames. At 10 kW, if the MLR is increased to 25% where the flame has almost no measurable soot, the visible length is the shortest among the flames studied. In this case the absence of soot luminosity makes the flame appear shorter. The 20 kW flames have a higher radiative fraction at a higher HLR. The 13% HLR flame has a more pronounced dip in the f_v at the center but the radial distribution is wider which indicates more total soot in the flame to provide luminosity for a longer flame. However, the high amount of soot also contributes to radiative cooling so that the flame length is not significantly different than that of the flame with a lower HLR.

Comparing the PDF deconvolution results to those obtained from average transmittances shows that the effects of turbulent fluctuations are

Conclusions

Among the factors influencing visible flame lengths of high liquid loading jet fires, soot temperature and volume fractions were investigated. Path integrated values of temperature were obtained and found to be steady. Local PDFs for soot volume fractions were found from the path integrated values, and the averages were compared to a simpler technique that neglects turbulent radiation interaction. As seen from the results, consideration of these interactions is important. The significant increase in soot volume fraction explains the increase in visible flame length with decreasing MLR.

References (Chapter 3)

1. Evans, D.D., Madrzykowski, D., and Haynes , G.A., *Fire Safety Science-- Proceedings of the Fourth International Symposium*, (T. Kashiwagi, Ed.) p. 1279.
2. Dutta, P., Gore, J.P., Sivathanu, Y.R., Sojka, P.E., *Combust. Flame.* 97:251-260 (1994).
3. Sivathanu, Y.R., and Gore, J.P., *Combus . Sci.Technol.* 76:45-66 (1991).
4. Sivathanu, Y.R.,Gore, J.P.,Janssen, J.M., and Senser, D.W., *J. Heat Transf.* 115:653-658 (1993)
5. Sivathanu, Y.R. and Gore, J.P., *JQSRT* 50, 483 (1993).
6. Sivathanu, Y.R. and Gore, J.P., *Combust. Flame* 94:265-270 (1993).

CHAPTER 4 SUMMARY, CONCLUSIONS AND FUTURE WORK

Various parameters that may affect the length of high liquid loading spray fires have been investigated. It was determined that although evaporation lengths do show the expected changes with firing rate, methane to liquid fuel ratio (MLR), and atomization quality, the magnitudes of the evaporation length and the variation are not large enough for the present atomization quality for this parameter to affect the visible flame length.

The radiative heat loss fraction data have shown that coupling between soot formation and energy loss due to radiation can lead to a variety of behavior with increasing heat release rates. For high MLR, the radiative heat loss fraction is primarily dominated by gas bands and appears to decrease with increasing firing rate. For intermediate MLRs, a behavior involving constant radiative heat loss fractions is observed. The radiative heat loss fraction for low MLRs increases with heat release rate reaches a maximum and then decreases with further increase in heat release rates. The visible flame lengths are strongly influenced by the soot formation, radiative heat loss and soot oxidation. Although, this is logical, existing flame length correlations do not account for radiative effects.

Scaling of the results from the present 10-20 kW heat release rate range to larger heat release rates needs to be considered in order to apply the results to practical fires. Fires up to 500 kW heat release rates can be studied in our laboratory. Buoyancy effects on the spray jet fires and changes in entrainment rates caused by the two phase flow effects also need examination. Whether the present findings concerning changes in soot luminosity with MLR and heat release rate are applicable to larger fires needs to be examined.

NIST-114
(REV. 6-93)
ADMAN 4.09

U.S. DEPARTMENT OF COMMERCE
NATIONAL INSTITUTE OF STANDARDS AND TECHNOLOGY

MANUSCRIPT REVIEW AND APPROVAL

(ERB USE ONLY)
ERB CONTROL NUMBER | DIVISION
PUBLICATION REPORT NUMBER: NIST-GCR-95-678 | CATEGORY CODE
PUBLICATION DATE: October 1995 | NUMBER PRINTED PAGES

INSTRUCTIONS: ATTACH ORIGINAL OF THIS FORM TO ONE (1) COPY OF MANUSCRIPT AND SEND TO THE SECRETARY, APPROPRIATE EDITORIAL REVIEW BOARD.

TITLE AND SUBTITLE (CITE IN FULL)

A Study of Two Phase High Liquid Loading Jet Fires

CONTRACT OR GRANT NUMBER: 60NANB3D1441

TYPE OF REPORT AND/OR PERIOD COVERED: 9/1/1993 - 8/30/1994

AUTHOR(S) (LAST NAME, FIRST INITIAL, SECOND INITIAL)
Wade, R., Sivathanu, Y.R. and J.P. Gore
School of Mechanical Engineering
Purdue University
West Lafayette, IN 47907-1077

PERFORMING ORGANIZATION (CHECK (X) ONE BOX)
[ ] NIST/GAITHERSBURG
[ ] NIST/BOULDER
[ ] JILA/BOULDER

LABORATORY AND DIVISION NAMES (FIRST NIST AUTHOR ONLY)
Building & Fire Research Laboratory/Fire Safety Engineering Division

SPONSORING ORGANIZATION NAME AND COMPLETE ADDRESS (STREET, CITY, STATE, ZIP)

PROPOSED FOR NIST PUBLICATION

[ ]	JOURNAL OF RESEARCH (NIST JRES)	[ ]	MONOGRAPH (NIST MN)	[ ]	LETTER CIRCULAR
[ ]	J. PHYS. & CHEM. REF. DATA (JPCRD)	[ ]	NATL. STD. REF. DATA SERIES (NIST NSRDS)	[ ]	BUILDING SCIENCE SERIES
[ ]	HANDBOOK (NIST HB)	[ ]	FEDERAL INF. PROCESS. STDS. (NIST FIPS)	[ ]	PRODUCT STANDARDS
[ ]	SPECIAL PUBLICATION (NIST SP)	[ ]	LIST OF PUBLICATIONS (NIST LP)	[X]	OTHER NIST-GCR
[ ]	TECHNICAL NOTE (NIST TN)	[ ]	NIST INTERAGENCY/INTERNAL REPORT (NISTIR)		

PROPOSED FOR NON-NIST PUBLICATION (CITE FULLY) [ ] U.S. [ ] FOREIGN

PUBLISHING MEDIUM
[ ] PAPER [ ] CD-ROM
[ ] DISKETTE (SPECIFY)
[ ] OTHER (SPECIFY)

SUPPLEMENTARY NOTES

ABSTRACT (A 2000-CHARACTER OR LESS FACTUAL SUMMARY OF MOST SIGNIFICANT INFORMATION. IF DOCUMENT INCLUDES A SIGNIFICANT BIBLIOGRAPHY OR LITERATURE SURVEY, CITE IT HERE. SPELL OUT ACRONYMS ON FIRST REFERENCE.) (CONTINUE ON SEPARATE PAGE, IF NECESSARY.)

High liquid loading spray jet fires occur in accidents involving fuel pipe leaks, tank ruptures and oil well blowouts. Laboratory simulations of such fires in the 10-30 kW range has recently become feasible using a novel effervescent atomizer burner. Measurements of flame length, radiative heat loss fractions, evaporation length, path integrated temperatures, and path integrated and local soot volume fractions in high liquid loading jet fires using this burner are reported. The data show that changes in evaporation length do not affect the flame length for the present operating conditions. The flame lengths increase with increasing heat release rate in an overall power law manner. Although the exit momentum for these flames is high, the power law behavior results from the effects of changes in radiative heat loss distribution with increasing firing rates. Increase in the mass flow rate of the atomizing methane from 5% to 25% causes a decrease in the soot volume fractions and an increase in the temperatures. The decrease in soot volume fraction and the increase in flame temperature have opposite effects on the visible flame length and radiative heat loss fraction.

KEY WORDS (MAXIMUM OF 9; 28 CHARACTERS AND SPACES EACH; SEPARATE WITH SEMICOLONS; ALPHABETIC ORDER; CAPITALIZE ONLY PROPER NAMES)

blowout fires; fire research; fuel sprays; flame length; flame temperature; heat release rate; methane; oil spills; radiative heat loss; soot; sprays

AVAILABILITY

[X] UNLIMITED [ ] FOR OFFICIAL DISTRIBUTION - DO NOT RELEASE TO NTIS
[ ] ORDER FROM SUPERINTENDENT OF DOCUMENTS, U.S. GPO, WASHINGTON, DC 20402
[X] ORDER FROM NTIS, SPRINGFIELD, VA 22161

NOTE TO AUTHOR(S): IF YOU DO NOT WISH THIS MANUSCRIPT ANNOUNCED BEFORE PUBLICATION, PLEASE CHECK HERE. [ ]

ELECTRONIC FORM